ISTANBUL TECHNICAL UNIVERSITY ★ INSTITUTE OF SCIENCE AND TECHNOLOGY

GENERALIZED FRACTAL DIMENSIONS AND INTERMITTENCY IN COUPLED MAP LATTICES

M. Sc. THESIS

Eng. M. N. Ayşe GORBON

Date of Submission	: 12 June 1995
Date of Approval	: 28 June 1995

Supervisor	: Doç. Dr. Ayşe ERZAN
Member	: Prof. Dr. Mahmut HORTAÇSU
Member	: Doç. Dr. Gazanfer ÜNAL

JUNE 1995

İSTANBUL TEKNİK ÜNİVERSİTESİ ★ FEN BİLİMLERİ ENSTİTÜSÜ

EŞLEMİŞ TASVİR ÖRGÜLERDE GENELLEŞTİRİLMİŞ FRAKTAL BOYUTLAR VE KESİKLİLİK

YÜKSEK LİSANS TEZİ

Fiz. Müh. M. N. Ayşe GORBON

Tezin Enstitüye Verildiği Tarih : 12 Haziran 1995

Tezin Savunulduğu Tarih : 28 Haziran 1995

Tez Danışmanı : Doç. Dr. Ayşe ERZAN

Jüri Üyeleri : Prof. Dr. Mahmut HORTAÇSU

: Doç. Dr. Gazanfer ÜNAL

HAZİRAN 1995

ACKNOWLEDGEMENT

I would like to thank to my supervisor, Doç. Dr. Ayşe ERZAN, who has shown all the interest that she can to help me and without whose help I would have never been able to complete this work. I am also grateful to her, since she has introduced me new concepts in physics, which I had never known that they existed.

TABLE OF CONTENTS

SUMMARY

In this thesis, we will be interested in how the wrinkledness of the graph of a system showing spatio–temporal intermittency is distributed. If the wrinkledness is not equally distributed, then the generalized dimensions of the graph, which are the scaling exponents of the moments of the averaged graph length, will have a nonlinear dependence on the moments, q. Moreover, if there is a Hölder condition on the solutions of the system, a relation between the generalized graph dimensions and the q^{th} order structure functions can be found. To understand how the non–uniformity of the wrinkledness of the graph is distributed, the generalized dimensions of the support are introduced. These dimensions are related with the generalized graph dimensions and the q^{th} order structure functions.

The systems we used to check the results are the coupled map lattices, which may be thought as simple replacements for non–linear partial differential equations. They are discrete in tme and space, and they are capable of displaying spatio–temporal chaos.

EŞLENMİŞ TASVİR ÖRGÜLERDE GENELLEŞTİRİLMİŞ FRAKTAL BOYUTLAR VE KESİKLİLİK

ÖZET

Çok serbestlik derecesine sahip, uzayda bir uzantısı olan sistemlerde, hem düzenli hem de düzensiz bölgelerin birarada bulundukları ve zaman içinde birlikte devindikleri bir bölge bulunur. Bu şekildeki davranışa uzay–zamansal kesiklilik adı verilir. Değişik uzay ve zaman bölgelerinde, farklı karmaşıklık derecelerine sahip bu davranışı tanımlayabilmek için sonsuz sayıda ölçeklenme üssüne ihtiyaç vardır ve böylece uzay–zamansal kesiklilik bir multifraktal dağılım olarak görülebilir.

Uzay–zamansal kesiklilik, nonlineer bir dönüşüme göre hareket eden ve deterministik kaos (düşük boyutlu karmaşık davranış) gösteren eşlenmiş elemanlara sahip bir sistem yardımıyla incelenebilir. Böyle bir sisteme örnek, eşlenmiş tasvir örgülerdir. Eşlenmiş tasvir örgüler kesikli uzay ve kesikli zamanda tanımlanırlar ve nonlineer tasvirin parametreleri ile eşlenme parametrelerine bağlı olarak bir faz değişimi gösterirler. Tam kritik bölgede, bazı domenler düzgün davranırken, bazıları kaotik davranır; yani sistem kesiklilik gösterir.

Tam gelişmiş türbülans da uzay–zamansal kesikliliğe bir örnektir. Bu konuda yapılan çalışmalarda, hidrodinamik hız alanlarının yapı fonksiyonlarının

$$\lim_{r \to 0} \left\langle \, |\vec{u}(\vec{x} + \vec{r}) - \vec{u}(\vec{x})|^q \, \right\rangle \sim r^{q\zeta_q}$$

şeklinde ökçeklendiği gösterilmiş ve üçüncü mertebe ölçeklenme üssü, ζ_3, $1/3$ olarak bulunmuştur. Bu denklemde, $< \cdots >$ uzay ve zaman üzerinden bir ortalamayı temsil etmektedir. Deneyler, bu üslerin, artan q değerleriyle birlikte, öngörülen değerlerden ($\zeta_q = 1/3$) sapmaya uğradıklarını ortaya koymuştur. Bu sapmaları açıklayabilmek için bir çok fraktal ve multifraktal model ileri sürülmüş, ancak bunların hidrodinamik türbülansı tanımlayan nonlineer kısmi diferansiyel denklemlerle (Navier–Stokes denklemleri) doğrudan bir ilişkileri olduğu gösterilememiştir.

Hidrodinamik alanların grafikleri ve bu grafiklerin alanların yapı fonksiyonlarının ölçeklenme davranışlarını tanımlayan geometrileri üzerine de

çalışmalar yapılmıştır. Girdaplılık alanının, $\vec{w} = \vec{\nabla} \times \vec{u}$, geometrik özellikleri incelenmiştir. Eş girdaplılık kümelerinin boyutları ve fraktal bir taşıyıcı üzerindeki girdaplılık konsantrasyonunun arasındaki ilişki ortaya konmuştur. Deneysel olarak, eş girdaplılık kümelerinin fraktal bir yapıya sahip oldukları gösterilmiş ve alanların grafiğinin kırışıklılığının bir ölçüsü olarak bir "grafik fraktal boyutu" tanımlanmıştır.

Eğer hidrodinamik türbülansı tanımlayan kısmi diferansiyel denklemlerin çözümleri üzerinde

$$G_\ell \leq \left\langle [1 + |\vec{\nabla} \cdot \vec{u}|^2]^{1/2} \right\rangle_{r_0} \sim r_0^h$$

şeklinde bir Hölder koşulu varsa ve h sonlu bir sabitse, alanı belirleyen kısmı diferansiyel denklemlerden h ölçeklenme üssünü bulabiliriz. Yukarıdaki denklemde, G_ℓ grafiğin uzunluğu, $\vec{u}$ hız alanı ve r_0, ortalamanın alındığı ölçektir. Ayrıca, yapı fonksiyonu üssü, ζ_1, ve grafik boyutu olarak tanımlanan h ölçeklenme üssü arasında bir ilişki bulunabilir. Bu yolla, kısmi diferansiyel denklemlerle ölçeklenme teorisi arasında bir bağlantı kurulabilir.

Bu çalışmada, bir kısmi diferansiyel denklemden değil, uzay–zamansal kesiklilik gösteren bir eşlenmiş tasvir örgüden yola çıkarak, bu sistemi karakterize eden bir boyutlu alanların grafiğinin kırışıklılığını inceleyeceğiz.

Kullandığımız eşlenmiş tasvir örgü $1+1$ boyutludur ve en yakın komşu etkileşmelerine sahiptir. Bu çalışmada yayınımsal bir eşlenme ele alınmıştır:

$$x_i(n+1) = (1-\varepsilon) f[x_i(n)] + \frac{\varepsilon}{2}\{f[x_{i+1}(n)] + f[x_{i-1}(n)]\}$$

Burada i örgü noktalarını ve n kesikli zamanı ifade eder. $f(x)$ yerel devinim kuralıdır ve ε, [0,1] aralığında tanımlı eşlenme parametresidir. Yerel devinim kuralı olarak "değiştirilmiş çadır tasviri" ve "lojistik tasvir" ele alınmıştır.

Değiştirilmiş çadır tasviri,

$$f(x) = \begin{cases} rx & \text{if } 0 \leq x \leq 1/2 \\ r(1-x) & \text{if } 1/2 \leq x \leq 1 \\ x & \text{if } x \geq 1 \end{cases}$$

ile verilir. Burada $r > 2$ nonlineer tasvirin parametresidir. Eşlenmemiş tasvirde, $f(x)$, [0,1] aralığındayken kaotik davranış gösterir. Bu aralığın dışına çıktığı zaman ise, sabit bir noktaya takılır ve orada kalır. Böylece, her noktanın kaotik ve düzenli durumları birbirinden kolaylıkla ayrılabilir ve laminer ile türbülan bölgeler tanımlanabilir. Tasvirler eşlendiğinde ise, laminer bölgedeki bir noktanın, yanındaki komşularının türbülan olmasına bağlı olarak, türbülan aralığa kayma olasılığı ortaya çıkar. Kullandığımız eşlenmiş tasvir örgüde, kritik bölge, ε eşlenme parametresi ve r parametresinin değerlerine bağlıdır.

Lojistik tasvir ise,

$$f(x) = \lambda x(1 - x)$$

olarak tanımlanır. Buarada x [0,1], λ ise [0,4] aralığındadır. Eşlenmemiş tasvirin sabit noktaları, $\lambda > 3$ için, kararlılıklarını kaybederler ve sistem kaosa yol açan periyod çiftleme davranışını gösterir. Tasvirler eşlendiğinde, bazı bölgelerde, noktalar zaman içinde periyodik davranış gösterirken, bazı bölgelerde kaotik davranırlar. Bu çalışmada, periyodik harekete laminer, kaotik davranışa ise türbülan adını vereceğiz. Eşlenmiş tasvirde, $\lambda > 3.63$ için, en büyük Lyapunov üsteli, negatif ile pozitif değerler arasıda hızla değişir. Böylece, $3.63 < \lambda < 4$ aralığında, λ'daki ufak bir değişmenin sistemin laminer durumdan kaotik duruma atlamasına sebep olduğu kritik bir bölge oluşmaktadır.

Tek boyutlu alanlar olarak düşünebileceğimiz x_i değişkenlerindeki en büyük olası değişimleri üzerinde barındıran bir L ölçeği bulunduğundan, bu saker alanların i'e göre grafiklerinin kendine afin olduklarını varsayalım. Bu grafiklerin boyutlarını bulabilmek için, L aralıklarını ℓ boyunda aralıklara bölelim ($\ell \leq L$). ℓ aralığı içindeki k ve $(k+1)$'inci noktaların arasındaki uzunluk bir dik üçgenin hipotenüsü olarak düşünülürse, ℓ aralığı içinde kalan grafiğin boyu

$$G_\ell(i) = \sum_{k=i-\ell/2}^{i+\ell/2} \left[1 + \left\{\frac{L}{r/2}(x_{k+1} - x_k)\right\}^2\right]^{1/2}$$

ile bulunabilir. Burada $L/(r/2)$ faktörü, bu büyüklüğü boyutsuzlandırmak için gereklidir. i, ℓ boyundaki aralıkların orta noktasıdır. L aralığı içindeki bir ℓ boyunda aralıktaki ortalama grafik uzunluğu

$$\left\langle \frac{1}{N_\ell} \sum_i^{N_\ell} G_\ell(i) \right\rangle \sim \left(\frac{\ell}{L}\right)^{-\beta}$$

olarak ölçeklenmektedir. Burada $N_\ell = L/\ell$, L aralığındaki ℓ boyundaki aralıkların sayısıdır. $< \cdots >$ zaman ve bütün grafik üzerine yerleşmiş değişik L aralıkları üzerinden ortalamayı göstermektedir. Eğer grafiğin multifraktal özellikleri varsa, ölçeklenme üslerinin aralıktan aralığa değişmesi beklenir:

$$G_\ell(i) \sim \left(\frac{\ell}{L}\right)^{-\gamma_i}$$

Buradaki tekillik üssü, γ, ℓ boyundaki bir aralık içindeki kırışıklığıölçmektedir. Eğer γ büyükse, grafik bu ölçekte çok kırışıktır. Küçük γ değerleri içinse, grafik oldukça düzgündür. γ her aralıkta değiştiğine göre, ortalama grafik uzunluğunun, $\langle G_\ell \rangle$, momentleri alındığında, değişik γ değerleri seçilecektir.

$$\langle G_\ell^q \rangle = \left\langle \frac{1}{N_\ell} \sum_i^{N_\ell} G_\ell^q(i) \right\rangle \sim \left\langle \frac{1}{N_\ell} \sum_i^{N_\ell} \left(\frac{\ell}{L}\right)^{-\gamma_i q} \right\rangle$$

$$\sim \left(\frac{\ell}{L}\right)^{-q\beta(q)}$$

Burada $\beta(q)$, genelleştirilmiş grafik boyutlarıdır. q arttırıldığında, büyük γ değerlerine sahip aralıklardan toplama daha fazla katkı gelecek ve dolayısıyla, daha büyük $\beta(q)$ değerleri seçilecektir. Kritik bölgede nümerik hesaplamalar yapıldığında gerçekten de, $q' > q$ için, $\beta(q) < \beta(q')$ bulunmuştur. Ayrıca $\beta(q)$'nun q bağımlılığı nonlineerdir (Bkz. Tablo 2).

Kullandığımız sistemin yapı fonksiyonlarını incelemek amacıyla, yukarıda verilen denklemdeki $r_0 \to 0$ limitini, kesikli uzayda çalıştığımızdan dolayıalamamamıza rağmen, aralarında ℓ kadar mesafe bulunan x_i skaler alanlarının bir ölçeklenme davranışı bulunup bulunmadığını araştıralım. Böylece yapı fonksiyonlarını, aralarında ℓ ($\ell \ll L$) kadar mesafe bulunan iki örgü noktasındaki alanların farkının uzay ve zaman üzerinden ortalaması olarak tanımlayalım ve momentlerinin

$$S_\ell^q = \left\langle \frac{1}{N_\ell} \sum_i^{N_\ell} |x_{i+\ell} - x_i|^q \right\rangle \sim \left(\frac{\ell}{L}\right)^{q\zeta_q}$$

olarak ölçeklendiğini varsayalım. Yapı fonksiyonları ile genelleştirilmiş grafik boyutları arasında bir ilişki kurabilmek için, ℓ boyunda bir aralığın üzerindeki grafik parçasının, ℓ/L boyunda d boyutlu kaç tane kutuyla örtülebileceğine bakalım. Bu sayının $\frac{|x_{i+\ell} - x_i|}{(\ell/L)}$ olacağı açıktır. L uzunluğundaki aralığın üzerinde bulunan grafik parçasını örtmek için gereken kutu sayısı

$$N = \left(\frac{L}{\ell}\right)^d \frac{|x_{i+\ell} - x_i|}{(\ell/L)}$$

olur. Ortalama grafik uzunluğunun, grafiği örtmek için gereken ortalama kutu sayısına eşit veya bu sayıdan daha büyük olması gerekir. Ortalama grafik uzunluğunun $(\ell/L)^{-\beta(1)}$ olarak ölçeklendiği hatırlanırsa,

$$\begin{aligned} \left(\frac{\ell}{L}\right)^{-\beta(1)} &\geq \left(\frac{L}{\ell}\right)^{d+1} \langle |x_{i+\ell} - x_i| \rangle \\ &\geq \left(\frac{\ell}{L}\right)^{\zeta_1 - d - 1} \end{aligned}$$

olduğu görülür. Buradan,

$$\beta(1) \leq d + 1 - \zeta_1$$

bulunur. Eğer grafik uzayı dolduracak kadar kırışıksa, $\beta(1)$, $d + 1$'e yaklaşacak ve ζ_1 sıfıra gidecektir. Öte yandan, grafik oldukça düzgünse, $\beta(1)$, d olacak ve dolayısıyla $\zeta_1 = 0$ olarak bulunacaktır. Yani, ζ_1 ölçeklenme üssü, alanın bir noktadan diğerine ne kadar düzgün veya düzgün olmayan bir şekilde değiştiğinin bir ölçüsünü vermektedir.

Genelleştirilmiş grafik boyutları ile q'uncu mertebeden yapı fonksiyonlarının arasındaki ilişkiyi bulmak için de aynı yöntem kullanılabilir. Ortalama grafik uzunluğunun momentleri, grafiği örtmek için gereken

ortalama d boyutlu kutu sayısının momentlerine eşit veya onlardan büyük olmalıdır. Böylece,

$$\left(\frac{\ell}{L}\right)^{-q\beta(q)} \geq \left(\frac{L}{\ell}\right)^{q(d+1)} \left\langle |x_{i+\ell} - x_i|^q \right\rangle$$
$$\geq \left(\frac{\ell}{L}\right)^{q(\zeta_- d-1)}$$

ve

$$\beta(q) \leq d + 1 - \zeta_q$$

bulunur. Kullandığımız sistemde $d = 1$ olduğundan,

$$\beta(q) \leq 2 - \zeta_q$$

elde ederiz. Nümerik olarak ζ_q ve $\beta(q)$ için bulunan değerler yerine koyulduğunda, bu eşitsizliğin sağlandığı, ancak hiçbir zaman eşitlik olarak doğrulanmadığı görülmektedir.

Daha önce, $\beta(q)$ değerlerinin q ile nonlineer olarak değişmesine bakarak, grafikteki kırışıklığın düzgün olarak dağılmadığı söylenmişti. Bu düzensizliğin nasıl dağıldığını anlamak için, korunan bir ölçü tanımlayalım:

$$\mu_i(\ell) = \frac{G_i(\ell)}{G_{tot}}$$

Burada, G_{tot} L uzunluğundaki bir aralıktaki toplam grafik uzunluğudur ve $\sum_i \mu_i = 1$. Bölüşüm fonksiyonunu

$$\chi_\ell(q) = \left\langle \sum_i \mu_i^q(\ell) \right\rangle$$

olarak tanımlayalım ve

$$\chi_\ell(q) \sim \left(\frac{\ell}{L}\right)^{\tau(q)}$$

şeklinde ölceklendiğini varsayalım. Burada, genelleştirilmiş boyut, $D(q)$, $\tau(q) = (q-1)D(q)$ ile verilir. $q = 0$ için, bölüşüm fonksiyonu ℓ boyundaki aralığı örtmek için gereken kutu sayısına indirgenir, yani $D(q = 0)$, grafiğin desteğinin boyutudur. Enformasyon boyutu, $D(1)$, μ ölçüsünün çoğunlukla üzerine yaşadığı kümenin boyutunu verir:

$$D(1) = \frac{\left\langle \sum_i \mu_i \ln \mu_i \right\rangle}{\ln \ell/L}$$

Eğer bütün kutularda aynı ölçü bulunuyorsa, $D(1)$, $D(0)$'a eşit olacaktır.

Eğer kırışıklığın çoklu ölçeklenme (multiscaling) özelliği varsa, genelleştirilmiş boyutlar bir aralıktan diğerine değişecektir. Bir tekillik üssü, α, tanımlayalım:

$$\mu_i(\ell) = \left(\frac{\ell}{L}\right)^{\alpha_i}$$

α tekillik üssü, daha önce tanımlanan γ tekillik üssüne benzemektedir. Buradan,

$$\chi_\ell(q) = \sum_i \mu_i^q(\ell) = \sum_i \left(\frac{\ell}{L}\right)^{\alpha_i q}$$
$$\sim \left(\frac{\ell}{L}\right)^{(q-1)D(q)}$$

olduğu görülebilir. q arttırıldığında, toplama, daha küçük α değerlerine sahip aralıklardan daha fazla katkı gelecek ve daha küçük $D(q)$ değerleri elde edilecektir. $q < 0$ için ise, grafiğin daha düzgün olan kısımlarına karşılık gelen büyük α değerleri toplama daha fazla katkıda bulunacak ve $D(q)$ değerleri artacaktır. Nümerik hesaplamalarda, kritik bölgede, $D(q)$ değerlerinin $q > 0$ için azaldığı, $q < 0$ içinse arttığı gözlenmiştir (Bkz. Tablo 3). Tamamiyle türbülan bölgede $\chi_\ell(q)$ için bir ölçeklenme sözkonusu olmadığından, $D(q)$ tanımlanamamaktadır. Laminer bölgede $D(q) = D(0) = 1$ bulunmuştur.

Tekillik üslerinin dağılımı, doğrudan genelleştirilmiş boyutlardan hesaplanabilir. Eğer, $N_\alpha(\ell)$, ölçünün α tekillik üslerine sahip olduğu aralıkların sayısı ise, bu S_α alt kümesiyle bir $f(\alpha)$ boyutunu ilişkilendirebiliriz.

$$N_\alpha(\ell) \sim \left(\frac{\ell}{L}\right)^{-f(\alpha)}$$

$\sum_i \mu_i^q(\ell)$ toplamı, bir aynı α tekilliğini taşıyan bütün kutular, (S_α), üzerinden alt toplamlara bölünürse,

$$\chi_\ell(q) = \sum_\alpha \sum_{S_\alpha} \left(\frac{\ell}{L}\right)^{\alpha q} = \sum_\alpha \left(\frac{\ell}{L}\right)^{\alpha q} N_\alpha(\ell)$$
$$= \sum_\alpha \left(\frac{\ell}{L}\right)^{\alpha q - f(\alpha)} \sim \int \left(\frac{\ell}{L}\right)^{\alpha q - f(\alpha)} d\alpha$$

olarak bulunabilir. Küçük (ℓ/L) değerleri için, integralde üslerin en küçüğü baskın olacağı için, bir eyer noktası yaklaşımı yapılabilir ve

$$\tau(q) = q\alpha(q) - f(\alpha(q))$$
$$\frac{\partial f(\alpha)}{\partial \alpha} = q$$
$$\frac{\partial \tau(q)}{\partial q} = \alpha(q)$$

bulunur. Bu, $\tau(q)$ fonksiyonundan $f(\alpha)$ boyutlarına bir Legendre dönüşümüdür. Bu dönüşüm kullanılarak, genelleştirilmiş boyutlardan $f(\alpha)$ değerleri kolaylıkla bulunabilir.

L aralığı içindeki toplam grafik uzunluğu, G_{tot},

$$G_{tot} = \left(\frac{L}{\ell}\right)^{d} \langle G_\ell \rangle = \left(\frac{L}{\ell}\right)^{d} \left(\frac{\ell}{L}\right)^{-\beta(1)} = \left(\frac{\ell}{L}\right)^{-d-\beta(1)}$$

olarak bulunur. Burada d, uzayın boyutudur. Böylece, korunan ölçü $\mu_i(\ell)$

$$\mu_i(\ell) \leq \frac{(\ell/L)^{-\gamma_i}}{(\ell/L)^{-d-\beta(1)}} \leq \left(\frac{\ell}{L}\right)^{d+\beta(1)-\gamma_i}$$

olarak yazılabilir. Genelleştirilmiş boyutları yeniden yazarsak,

$$\left(\frac{\ell}{L}\right)^{(q-1)D(q)} \leq \left\langle \sum_i \mu_i^q(\ell) \right\rangle = \left\langle \sum_i \left(\frac{\ell}{L}\right)^{q[d+\beta(1)-\gamma_i]} \right\rangle$$

buluruz. $(\ell/L)^{[d+\beta(1)]q}$ büyüklüğü ortalamanın dışına alınırsa,

$$\begin{aligned} \left(\frac{\ell}{L}\right)^{(q-1)D(q)} &\leq \left(\frac{\ell}{L}\right)^{q[d+\beta(1)]} \left\langle \sum_i \left(\frac{\ell}{L}\right)^{q-\gamma_i} \right\rangle \\ &\leq \left(\frac{\ell}{L}\right)^{q[d+\beta(1)]-[d+q\beta(q)]} \end{aligned}$$

bulunur. Buradan,

$$D(q) \leq \frac{q}{q-1}[\beta(1) - \beta(q)] + d$$

elde edilir. Kullandığımız sistemde $d = 1$ olduğundan, bu eşitsizlik

$$D(q) \leq \frac{q}{q-1}[\beta(1) - \beta(q)] + 1$$

halini alır. $\beta(q)$ ve $D(q)$ için bulunan değerler bu denkleme yerleştirildiğinde, eşitsizliğin gerçeklendiği görülmektedir.

Yukarıdaki denkleme, genelleştirilmiş grafik boyutları ile yapı fonksiyonları arasında bulunmuş olan eşitsizlik yerleştirilirse,

$$D(q) \leq \frac{q}{q-1}[\zeta_q - \zeta_1] + 1$$

eşitsizliği elde edilir. Yine bu denklemde ζ_q ve $D(q)$ için bulunan değerler yerine yerleştirilirse, eşitsizliğin sağlandığı, ancak, beklenileceği gibi, eşitlik olarak doğrulanmadığı görülmektedir (Bkz. Tablo 2,3).

CHAPTER 1. INTRODUCTION

Many structures in nature, such as mountains, rivers, clouds, lightning, etc., are highly irregular and fragmented. Many of these structures can be shown to be scale–invariant, or in other words, their irregularity is identical on all scales. These kind of structures are named fractals [1]. Fractals can be characterized by a scaling index called the fractal dimension.

1.1. Fractal and Multifractal Measures

One of the parameters to characterize a structure geometrically is the dimension. The dimension can be defined in many ways, but generally, they all give the same result. To characterize irregular structures, the box dimension can be used [1]. Let us take a set S and divide it into ε–sized boxes. The box dimension, then, is given by,

$$D_B = \lim_{\varepsilon \to 0} \frac{\ln N(\varepsilon)}{\ln(1/\varepsilon)} \tag{1.1}$$

where $N(\varepsilon)$ is the minimum number of d–dimensional boxes of size ε, needed to cover all the points of the set S. For most cases of interest, the box dimension is equal to the Hausdorff dimension [2]. If we again cover a set S by d–dimensional boxes of sizes $\{\varepsilon_i\}$, the Hausdorff dimension, D_H, is defined as the critical dimension for which the Hausdorff measure, $H_d(\varepsilon)$, takes a finite value:

$$H_d(\varepsilon) = \lim_{\varepsilon \to 0} \inf \sum_i \varepsilon_i^d \to \begin{cases} 0, & \text{if } d > D_H \\ \text{finite}, & \text{if } d = D_H \\ \infty, & \text{if } d < D_H \end{cases} \tag{1.2}$$

where the infimum is taken over all possible coverings with the constraint $\varepsilon_i \leq \varepsilon$. The set is called a fractal if its Hausdorff dimension exceeds its topological dimension (the number of linearly independent directions in which one an move around a given point of the set S). In this study, we are going to take the fractal dimension $D_F = D_B$.

Some fractal measures may require an infinite set of scaling indices, and are called multifractal measures. For multifractals, the q^{th} moment of the measure scales with an exponent that has a nonlinear dependence on q. Multifractals have been shown to exist in dynamical systems [3–6], in fully developed turbulence [7], in the statistical mechanics of disordered systems [7]. Multifractals scale as,

$$\chi_\ell(q) = \sum_i \mu_i^q(\ell) \sim \ell^{\tau(q)} \tag{1.3}$$

where $\chi_\ell(q)$ is the partition function; $\mu_i(\ell)$ is the multifractal measure ($\sum_i \mu_i(\ell) = 1$), and ℓ is the size of the d–dimensional boxes needed to cover the set S. The sum runs over the different boxes of size ℓ on which the measure μ lies.

1.2. Spatio–Temporal Intermittency

In spatially extended systems with many degrees of freedom, there exists a regime where both regular and chaotic domains coexist, and evolve in space–time. This behavior is called spatio–temporal intermittency. To characterize this behavior with different degrees of complexity over different spatial and temporal domains requires an infinite set of exponents, and thus multifractality arises naturally in the concept of spatio–temporal intermittency.

Fully developed turbulence (FDT) is one of the most significant examples of spatio–temporal chaos. The property of FDT that attracted

most attention is the scaling behavior of the velocity field. The scaling behavior was first pointed out by Richardson [8], and later worked out by Kolmogorov [9] and Obukhov [10]. They proposed a set of hypothesis about the nature of high–Reynolds number turbulence, and predicted that the fluid velocity field should be self–similar over a wide range of scales, such that

$$\left\langle |\vec{u}(\vec{x}+\vec{r}) - \vec{u}(\vec{x})|^q \right\rangle \sim r^{q\zeta_q} \tag{1.4}$$

They have found the third order scaling exponent, ζ_3 to be $1/3$. However, even though this value is compatible with experimental results, higher order structure functions deviate from Kolmogorov's prediction ($\zeta_q = 1/3$) experimentally [11]. This deviation has given rise to a large number of models based on fractal or multifractal models. Kolmogorov [8] assumes that the energy dissipation is smoothly distributed in space and the average dissipation is conserved at every step of the cascade. Mandelbrot [12] preserves the same cascade model. but in his hypothesis (called the β–model or absolute curdling) the energy is conserved at each step, but does not fill all the space. Benzi et al. [13] argue in their multifractal model (called random β–model or weighted curdling) that the dissipation is distributed with a probability density. so that eddies with different dissipation rates are created. But there has not been found a connection between these models and the equations of hydrodynamics.

1.3. The Geometric Characterization of Turbulence and the Graph Dimension

Some other studies have been made on the graphs of the hydrodynamic field and the geometries of these graphs that determine the scaling behavior of the structure functions of the fields [14–17]. The geometrical properties of the field of vorticity magnitude, $\vec{w} = \vec{\nabla} \times \vec{u}$, which increases rapidly in some regions, have been studied. The connection between the

dimension of the level sets and the concentration of vorticity on a fractal carrier can be demonstrated [18]. Since the dimension of the level sets and the dimension of the graph of the field are related via Euler relation, this approach promised to be a route to connecting the fractal properties of the flow field to the differential equations of hydrodynamics.

We have already mentioned that the level sets in FDT may have fractal properties and a "graph fractal dimension" can be defined as a measure of wrinkledness of the graph of the field. Sreenivasan [19] has shown in his experiments, where he used a dye as a passive scaler in a turbulent jet, that the level sets are fractal.

If there is a Hölder condition on the solutions of the partial differential equation,

$$G_\ell \leq \left\langle [1 + |\vec{\nabla} \cdot \vec{u}|^2]^{1/2} \right\rangle \sim \ell^h \tag{1.5}$$

where G_ℓ is the length of the graph in an ℓ–sized interval, and h a finite constant, then we can estimate the exponent h from the partial differential equation governing the field. We can also find a relation between the structure function exponent ζ_1 and the scaling exponent h [20], which will be defined as the graph dimension. This is one way in which a direct connection between the partial differential equations and the scaling theory can be established.

1.4. Coupled Map Lattices

The coupled map lattices can be viewed as a simplified replacement for the partial differential equations arising in hydrodynamics and similar fields [21]. A CML is a system that is made up of a coupled array of elements which evolve according to a nonlinear transformation and are capable of displaying deterministic chaos (low dimensional chaotic behavior) [22–24]. A CML is, thus, a dynamical system with discrete time, discrete

space and continuous state, and it displays spatio–temporal chaos. The studies on CMLs indicate phase transitions similar to those in statistical physics. The transitions are dependent on the coupling parameter and the other parameters of the nonlinear map [25–27]. In the critical region, while some domains remain regular, some show chaotic behavior, and these domains change in the course of time in an irregular manner, that is, the system exhibits intermittency. The chaotic domains, seen in the $d+1$ dimensional space, form a fractal set at the critical parameters of the phase transition [26]. Numerical and analytical studies have shown that, at the critical region, scaling functions and critical exponents (that are dependent on the critical parameters) can be defined [24–26].

1.5. Outline of the Thesis

In Chapter 2, we have investigated if the wrinkledness of the graph of a CML has fractal properties. We have numerically computed the scaling exponent β (the graph dimension). Since the system is intermittent, we have assumed that the wrinkledness is not equally distributed, and defined the generalized graph dimensions, $\beta(q)$, as

$$\langle G_\ell^q \rangle \sim \left(\frac{\ell}{L}\right)^{q\beta(q)} \tag{1.6}$$

where G_ℓ is the length of the graph over an ℓ–sized interval, and L is the typical length over which the maximum possible variations in the field are registered. If there is an inhomogeneous distribution, $\beta(q)$ will depend on q. We have seen that this asumption is true.

In Chapter 3, we have worked out a relation between the generalized graph dimensions and the q^{th} order structure functions, which generalizes the relation that has been given for $q = 1$ [20]. When the numerical results are placed in the relation, we see that the inequality is satisfied, but not saturated.

In Chapter 4, to understand how the non–uniformity of the wrinkledness is distributed, we defined a conserved measure and computed the scaling exponents, $D(q)$, the generalized dimensions of the support of the graph. We have found that the information dimension, $D(1)$, the fractal dimension of the subset on which the bulk of the wrinkledness lives, is less than the fractal dimension of the substrate, $D(0)$. We have worked out a relation between $\beta(q)$ and $D(q)$, and saw that it is numerically verified. By applying a Legendre transform, we have also computed the dimensions, $f(\alpha(q))$, of the sets on which the parts of the graph with different singularity exponents, $\alpha(q)$, are concentrated.

In Chapter 5, we summarize our results.

CHAPTER 2. GENERALIZED FRACTAL DIMENSIONS ON COUPLED MAP LATTICES

2.1. The Coupled Map Lattice

As defined in Chapter 1, coupled map lattices (CML) are one of the ways to investigate spatio–temporal chaos. They are discrete in time and space, and they possess nearest–neighbor interactions. Although there are various kinds of couplings between nearby lattice points that can be used in a CML, in this study, we are going to use a CML with diffusive coupling:

$$x_i(n+1) = (1-\varepsilon)\, f[x_i(n)] + \frac{\varepsilon}{2}\left\{ f[x_{i+1}(n)] + f[x_{i-1}(n)] \right\} \qquad (2.1)$$

where i denotes the lattice site, and n shows the discrete time. The space dimension is 1. $f(x)$ is the local evolution rule and ε is the coupling parameter in the range [0,1]. We have taken two maps as examples for the local evolution rule: the modified tent map and the logistic map.

2.1.1. Modified Tent Map

The modified tent map is given by

$$f(x) = \begin{cases} rx, & \text{if } 0 \le x \le 1/2 \\ r(1-x), & \text{if } 1/2 \le x \le 1 \\ x & \text{if } x > 1 \,. \end{cases} \qquad (2.2)$$

with $r > 2$.

When we consider the uncoupled map, it is easily seen that, for large enough r, $f(x)$ shows chaotic behavior as long as the function is in the interval [0,1]. For $r > 2$, points within this interval eventually ecape into (1,$r/2$]. When the variable x is in (1,$r/2$], the iterations lock at a fixed point and remain there (Fig (2.1)). The regular and chaotic states of each point can be easily distinguished, and laminar and turbulent domains can be defined [25]. When the maps are coupled, however, there appears a possibility that a site in the laminar domain can end in the turbulent interval at the next iteration, depending upon its neighbors being turbulent.

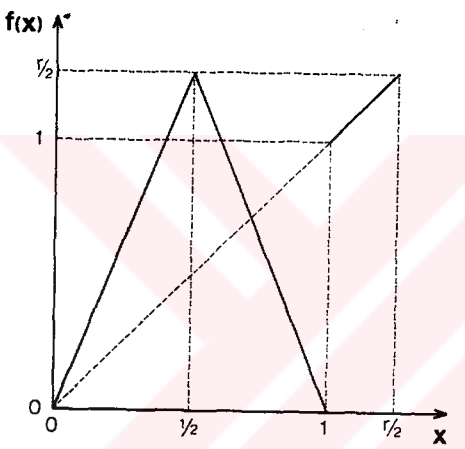

Fig. 2.1 The modified tent map.

In the CML we have used, the critical region depends on the values of both the parameter r and the coupling parameter ε. For different r values, there exist different critical coupling parameters, ε_c [25], as shown in Table (2.1). As $r \rightarrow 2$, the probability of a turbulent site escaping to the laminar region goes to zero. Also, when r is fixed, and ε is increased. the number of turbulent sites increase

Table 2.1. Critical coupling parameters for different r values [25].

r	ε_c
2.539	0.1
3	0.3593
3.735	0.7
3	0.9083

2.1.2. Logistic Map

The logistic map is given by

$$f(x) = \lambda x(1-x) \tag{2.3}$$

with x in the interval [0,1], and $0 \leq \lambda \leq 4$ (Fig. (2.2)). The fixed points of the uncoupled map lose their stability for $\lambda > 3$, and the system exhibits the period–doubling route to chaos. When the maps are coupled, there appears domains in some of which the points show a period–doubling behavior *in time*, and in some of which the evolution is chaotic [21] (Fig. (2.3). In this system, we are going to denote the periodic behavior as laminar, and the regions that behave chaotically as turbulent.

Recall that for $\lambda > 3.59$, the logistic map shows a transition to chaos. For the coupled map, it was found [28] that, around $\lambda \simeq 3.63$, the largest Lyapunov exponent from being negative to positive. For $\lambda > 3.63$, the largest Lyapunov exponent shows very erratic behavior, changing rapidly between negative and positive values. Thus the whole region $3.63 < \lambda < 4$ seems to be a critical region where a small change in λ drives the system

from being laminar to turbulent.

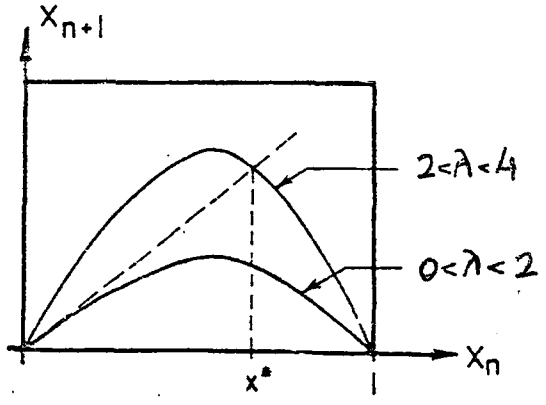

Fig. 2.2 The logistic map.

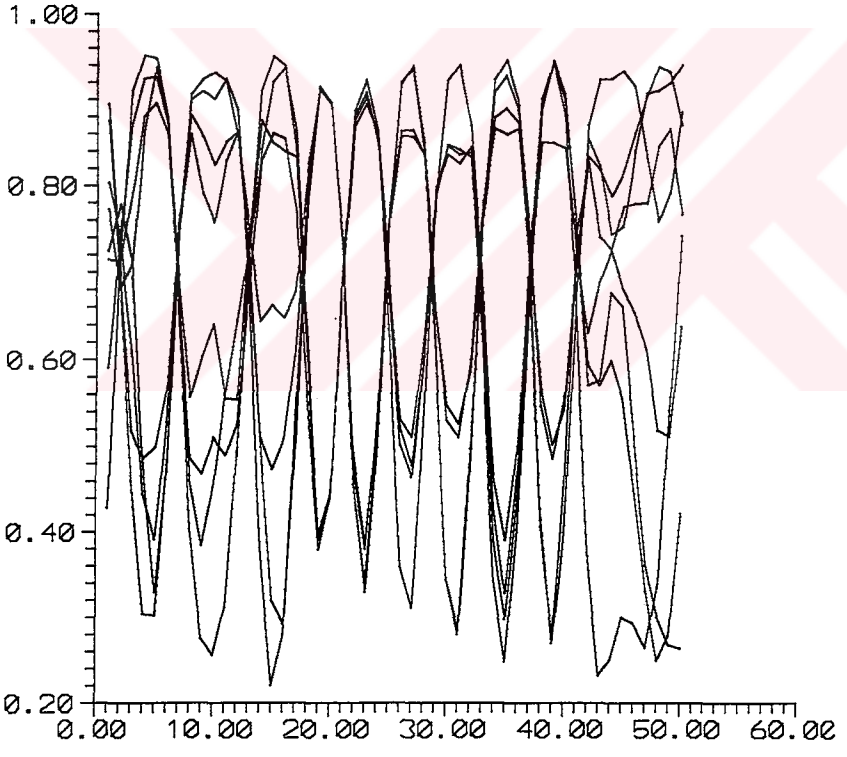

Fig. 2.3 Different time snapshots drawn together for the logistic map. One can easily see that the ponits have a periodic behavior in some regions, while in others they evolve chaotically.

map. One can easily see that the points have a periodic behavior in some regions, while in others they evolve chaotically.

2.2. The Generalized Dimensions of the Graph

We expect the graph of x_i vs i to be self–affine, that is, there exists a typical scale L, on which the largest possible variations in x_n are registered, and therefore the scaling behavior in the horizontal and the vertical directions are different (Figs. (2.4–5)).

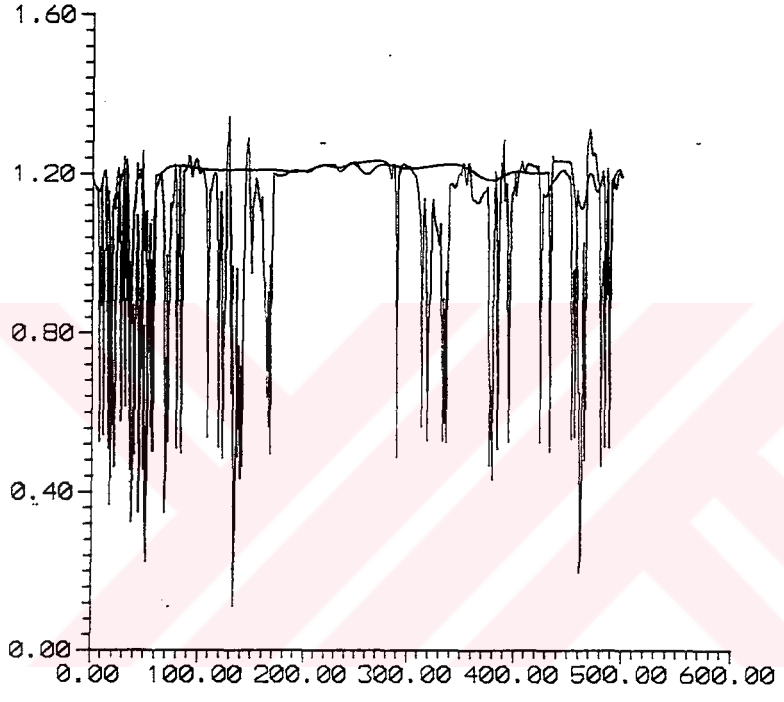

Fig. 2.4. The graph of the coupled modified tent map drawn at different time snaphots.

To find the dimension of the graph of x_n vs n on a lattice of N sites with periodic boundary conditions at any time step (after the transients die out), we have calculated the length of the graph, dividing the typical scale L into ℓ–sized intervals ($\ell \leq L$). If we consider the length of the graph between the k^{th} and $(k+1)^{st}$ sites to be the hypothenuse of a right triangle, then the length of this part is given by:

$$\Delta(k) = \left\{1 + \left[\{\frac{L}{(r/2)}\},(x_{k+1} - x_k)\right]^2\right\}^{1/2} \qquad (2.4)$$

where the scaling factor $\frac{L}{(r/2)}$ is needed to make this quantity dimensionless. The length of the graph over an L–sized interval is,

$$G_\ell(i) = \sum_{k=1-\ell/2}^{i+\ell/2} \Delta(k) \tag{2.5}$$

where i is the position of the midpoint of the interval of size ℓ. Then the length of the graph that can be fit into an ℓ–sized interval is

$$\sum_{i=1}^{N_\ell} G_\ell(i) \tag{2.6}$$

where $N_\ell = L/\ell$. Averaging over different snapshots and different L placements, one finds

$$\left\langle \frac{1}{N_\ell} \sum_{i=1}^{N_\ell} G_\ell(i) \right\rangle \sim \left(\frac{\ell}{L}\right)^{-\beta} \tag{2.7}$$

Here, $< \cdots >$ denotes averaging both over time and space with respect to the Lebesgue measure. If the graph has multiscaling properties, we expect the scaling exponents to vary from one interval to another. So, we define a singularity exponent, γ, as

$$G_\ell(i) \sim \left(\frac{\ell}{L}\right)^{-\gamma_i} \tag{2.8}$$

The singularity exponent is a measure of the wrinkledness over an L–sized interval. If γ is big, the graph will be highly wrinkled at all scales, and if γ is small, it will be quite smooth. As ℓ is narrowed down, the number of balls needed to cover the graph grow drastically for $\gamma > 0$ and large. Since γ differs from interval to interval, when moments of the average graph length, $\langle G_\ell \rangle$, are taken, different γ values will be chosen.

$$\begin{aligned} \left\langle G_\ell^q \right\rangle &= \left\langle \frac{1}{N_\ell} \sum_{i=1}^{N_\ell} G_\ell^q(i) \right\rangle \\ &\sim \left\langle \frac{1}{N_\ell} \sum_{i=1}^{N_\ell} \left(\frac{\ell}{L}\right)^{-\gamma_i q} \right\rangle \sim \left(\frac{\ell}{L}\right)^{-q\beta(q)} \end{aligned} \tag{2.9}$$

Here, $< \cdots >$ has the same meaning as before. When q is increased, the parts that have a big value of γ will contribute more to the expectation value of the graph length. so bigger $\beta(q)$ values will be obtained.

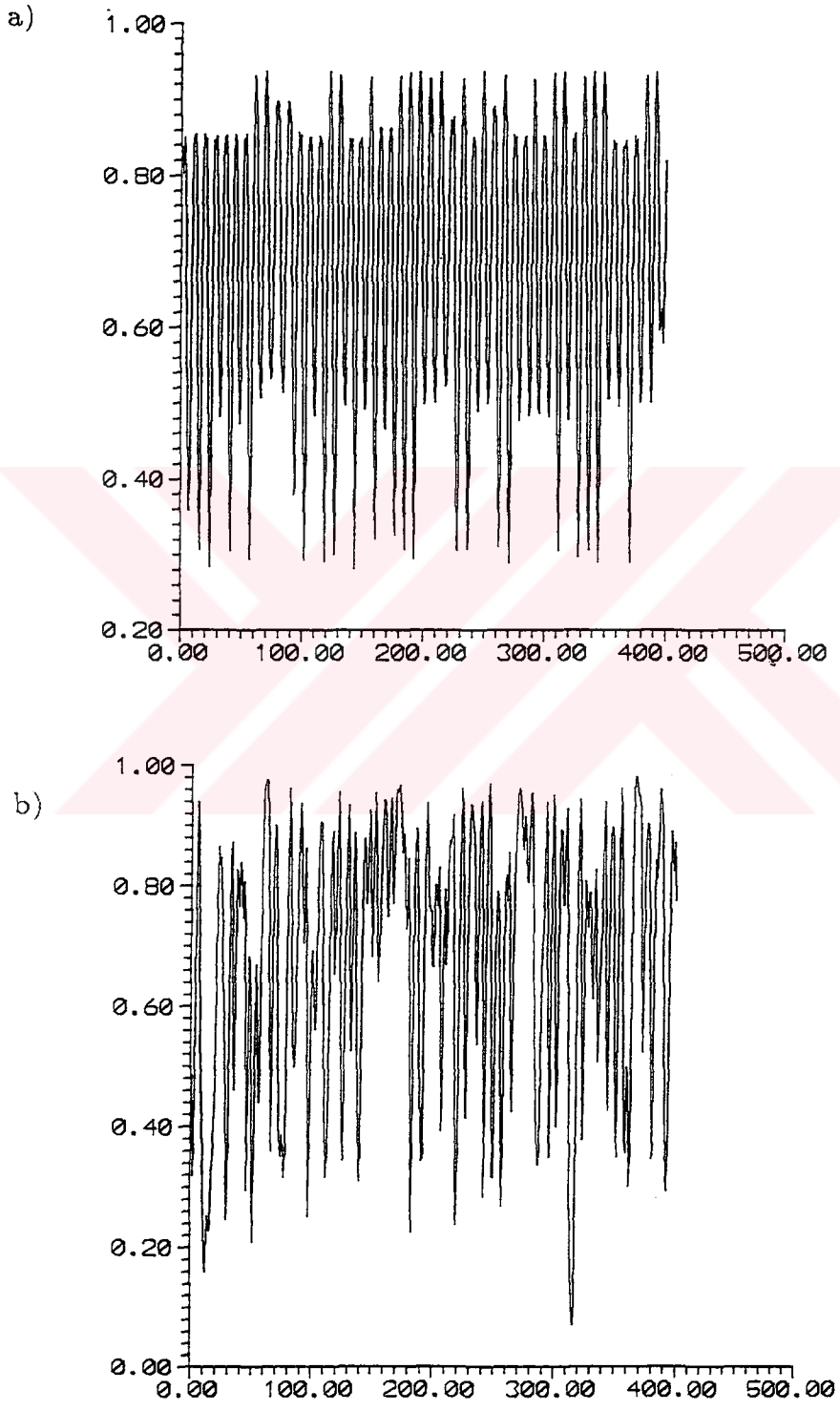

Fig. 2.5 The graph of the coupled logistic map taken at one time step for different λ values: a)$\lambda = 3.76$, b)$\lambda = 3.81$, d)$\lambda = 3.94$.

c)

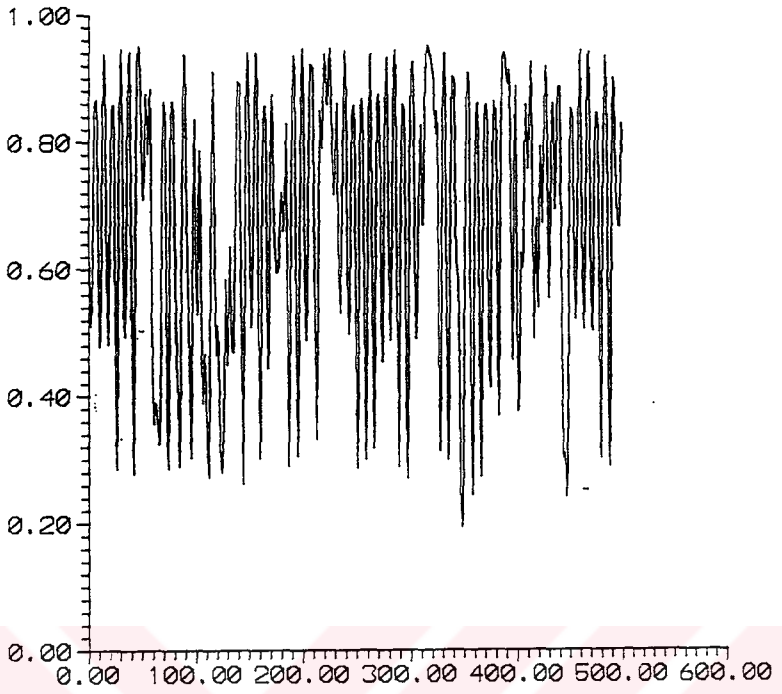

Fig. 2.5 The graph of the coupled logistic map taken at one time step for different λ values: a)$\lambda = 3.76$, b)$\lambda = 3.81$, d)$\lambda = 3.94$ (continued).

2.3. Computation

To show the scaling behavior of the expectation value of the graph length, we have computed the generalized graph dimensions for different values of r and ε_c (Figs. (2.6)–(2.7)), and we have seen that $\beta(q)$ increases as q increases. Moreover this dependence on q is nonlinear. The results are given in Table (2.2) for the modified tent map, and in Table (2.3) for the logistic map. The q dependence of $\beta(q)$ is shown in Fig. (2.8) and (2.9).

Table 2.2. $\beta(q)$ values for different ε_c and r parameters in the modified tent map.

$\beta(q)$	$\varepsilon_c = .1$ $r = 2.539$	$\varepsilon_c = .3591$ $r = 3$	$\varepsilon_c = .7$ $r = 3.735$	$\varepsilon_c = .9083$ $r = 3$
$\beta(0)$	1.12±.03	1.13±.04	1.09±.04	1.19±.06
$\beta(1)$	1.21±.07	1.18±.07	1.12±.08	1.26±.09
$\beta(2)$	1.3±.1	1.2±.1	1.14±.07	1.4±.1
$\beta(3)$	1.4±.1	1.3±.1	1.16±.09	1.4±.1
$\beta(4)$	1.5±.1	1.4±.2	1.2±.1	1.5±.1
$\beta(5)$	1.59±.08	1.4±.1	1.2±.1	1.6±.1

Table 2.3. $\beta(q)$ values for different λ values in the logistic map.

$\beta(q)$	$\lambda = 3.71$	$\lambda = 3.76$	$\lambda = 3.81$	$\lambda = 3.94$
$\beta(0)$	1.42±.08	1.52±.08	1.51±.08	1.57±.7
$\beta(1)$	1.43±.08	1.53±.08	1.52±.08	1.58±.08
$\beta(2)$	1.44±.09	1.5±.1	1.53±.08	1.58±.09
$\beta(3)$	1.4±.1	1.5±.1	1.5±.1	1.6±.1
$\beta(4)$	1.4±.1	1.5±.2	1.5±.1	1.6±.1

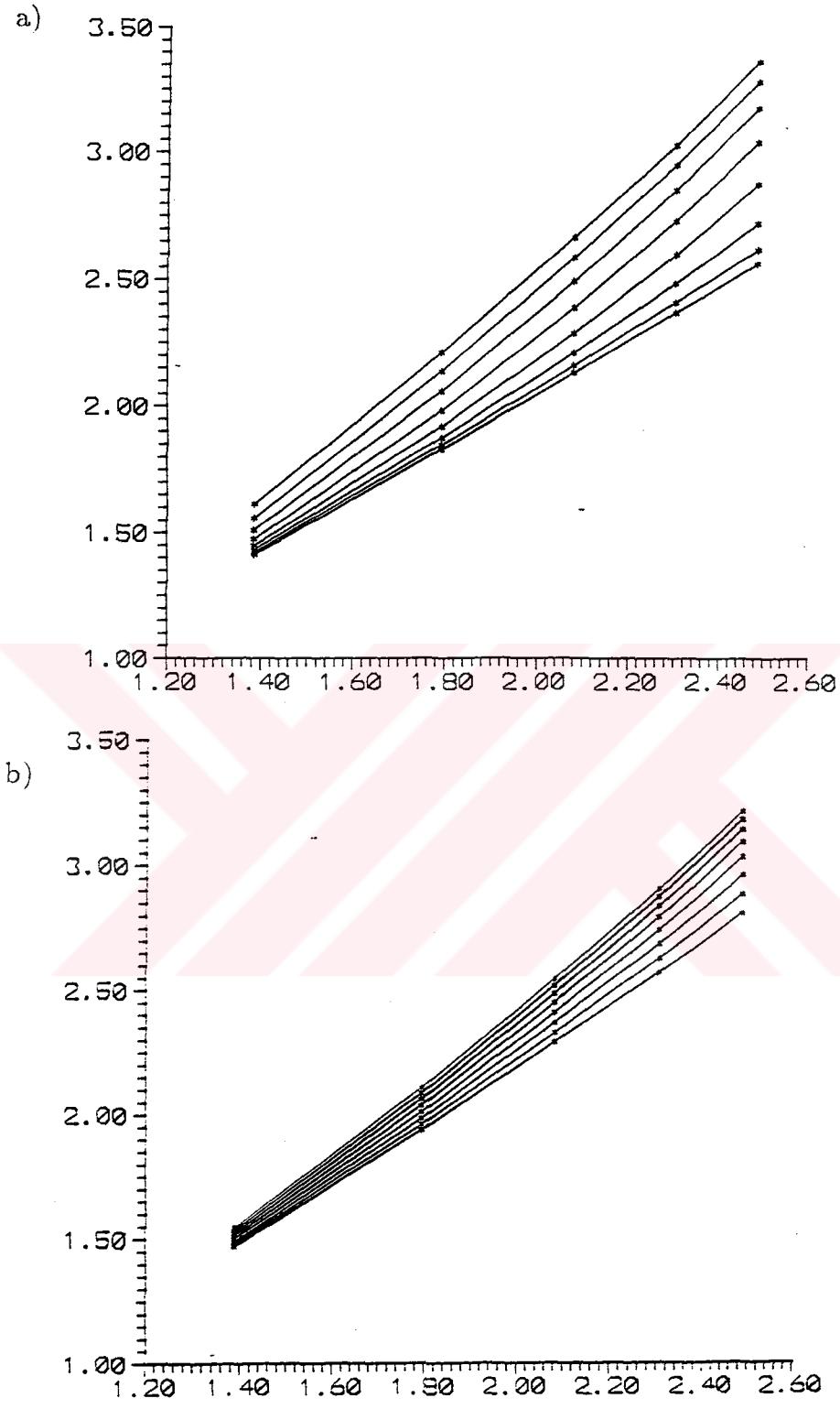

Fig. 2.6. The scaling behavior of the moments of the averaged graph length, $< G_\ell^q >$, for different r and ε_c parameters in the modified tent map: a)$r = 2.539$, $\varepsilon_c = 0.1$, b)$r = 3$, $\varepsilon_c = 0.3593$, c)$r = 3.735$, $\varepsilon_c = 0.7$, d)$r = 3$, $\varepsilon_c = 0.9983$.

c)

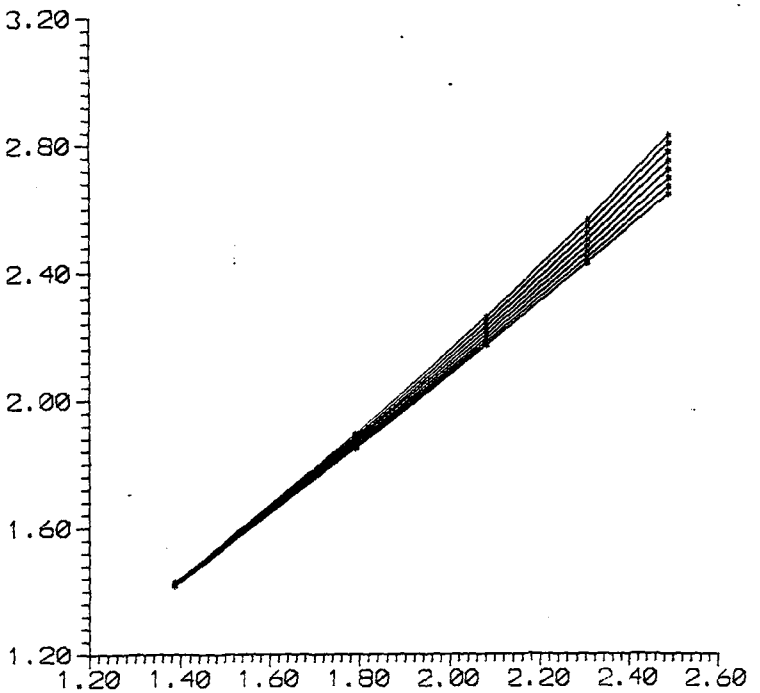

d)

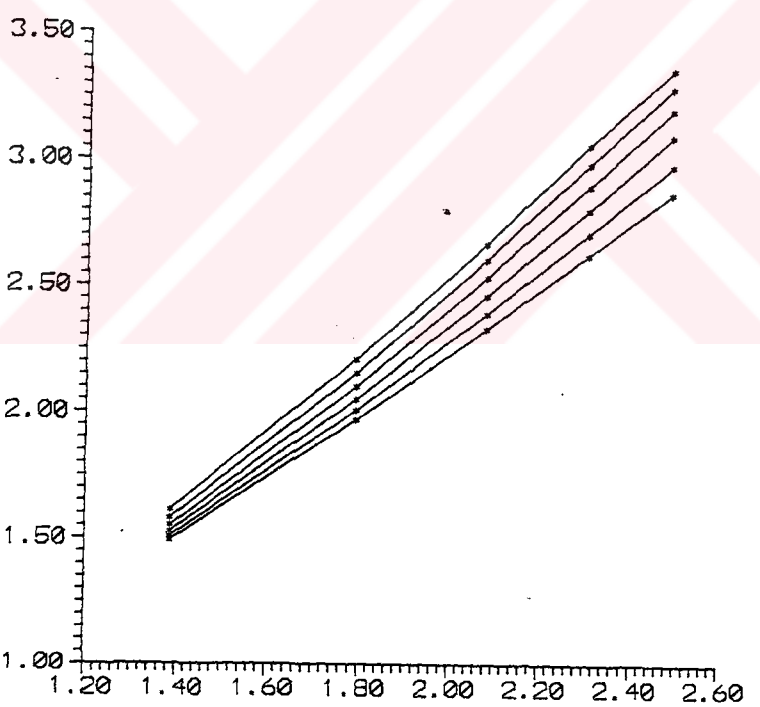

Fig. 2.6. The scaling behavior of the moments of the averaged graph length, $< G_\ell^q >$, for different r and ε_c parameters in the modified tent map: a)$r = 2.539$, $\varepsilon_c = 0.1$, b)$r = 3$, $\varepsilon_c = 0.3593$, c)$r = 3.735$, $\varepsilon_c = 0.7$, d)$r = 3$, $\varepsilon_c = 0.9983$ (continued).

a)

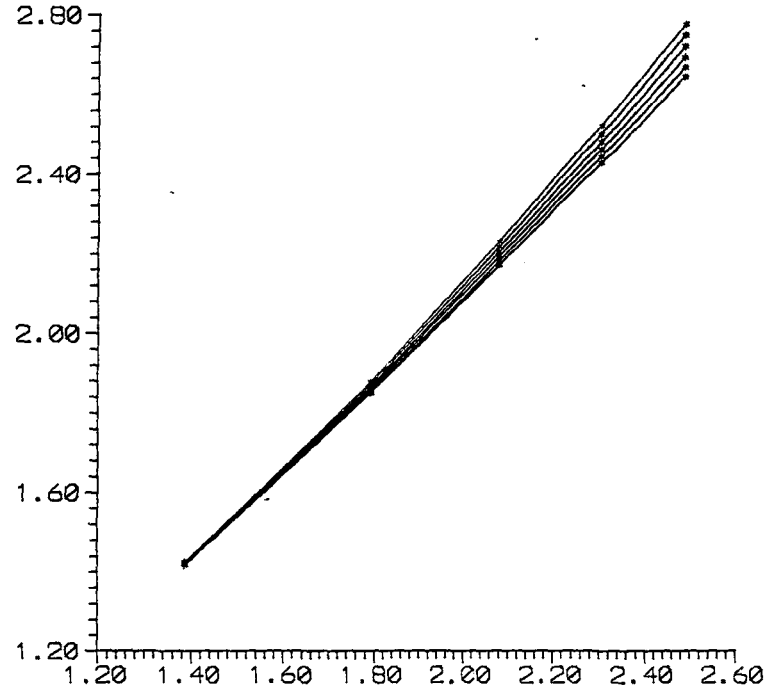

b)

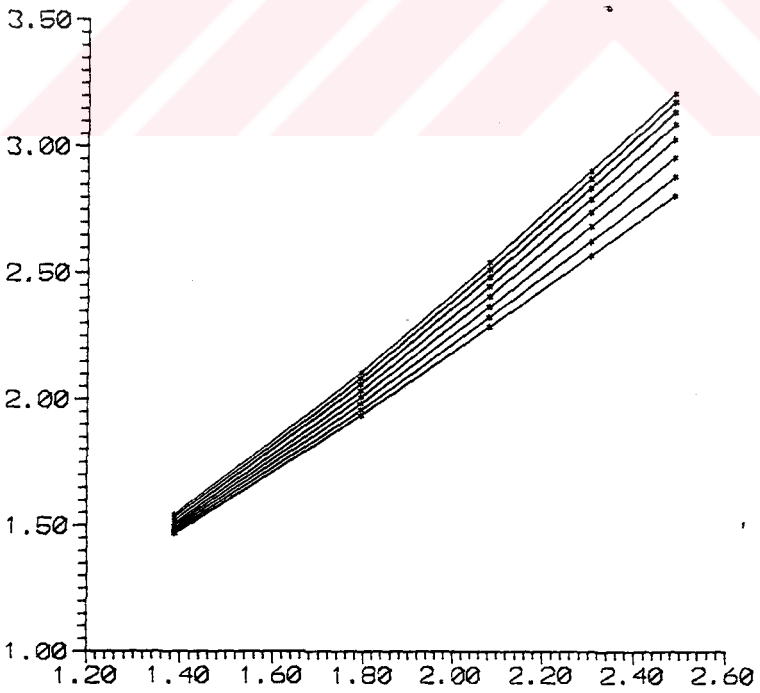

Fig. 2.7 The scaling behavior of the moments of the averaged graph length, $< G_\ell^q >$, for different λ values: a)$\lambda = 3.71$, b)$\lambda = 3.76$, c)$\lambda = 3.81$, d)$\lambda = 3.94$.

c)

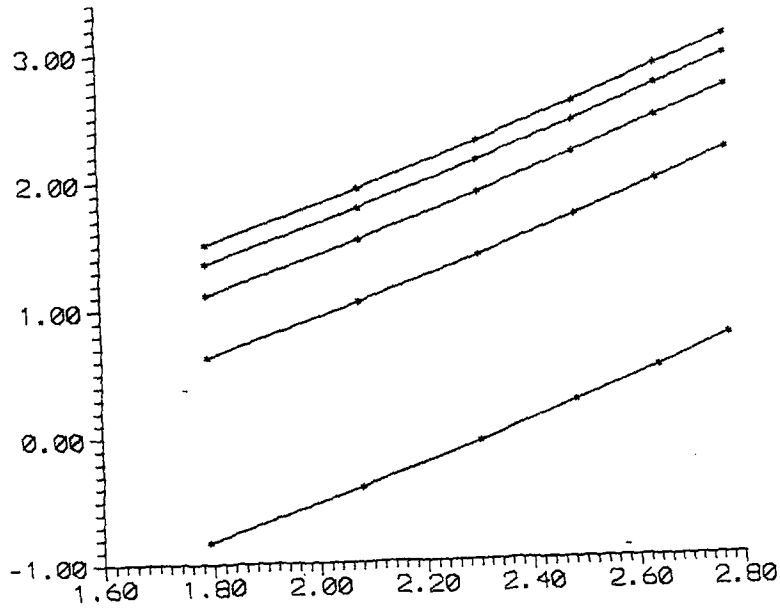

d)

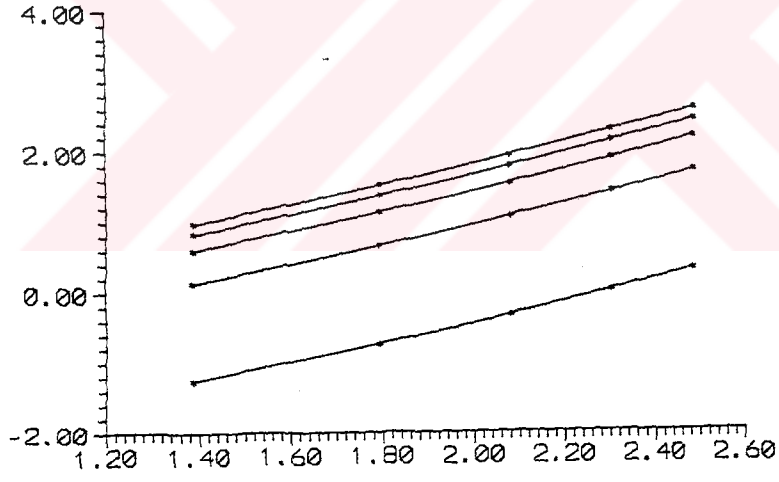

Fig. 2.7 The scaling behavior of the moments of the averaged graph length, $< G_\ell^q >$, for different λ values: a)$\lambda = 3.71$, b)$\lambda = 3.76$, c)$\lambda = 3.81$, d)$\lambda = 3.94$ (continued).

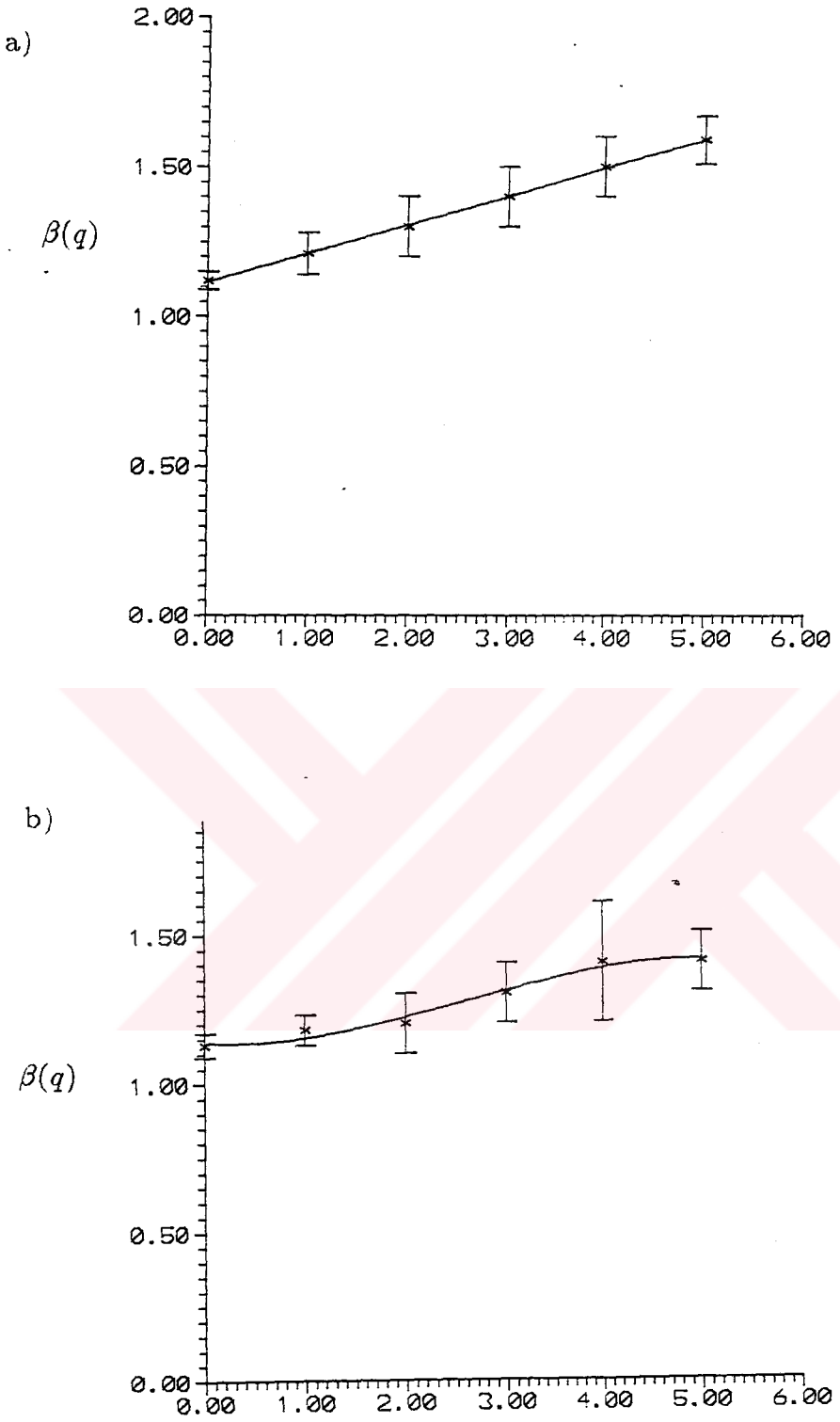

Fig. 2.8. $\beta(q)$ vs. q for the modified tent map: a)$r = 2.539$, $\varepsilon_c = 0.1$, b)$r = 3$, $\varepsilon_c = 0.3593$, c)$r = 3.735$, $\varepsilon_c = 0.7$, d)$r = 3$, $\varepsilon_c = 0.9983$.

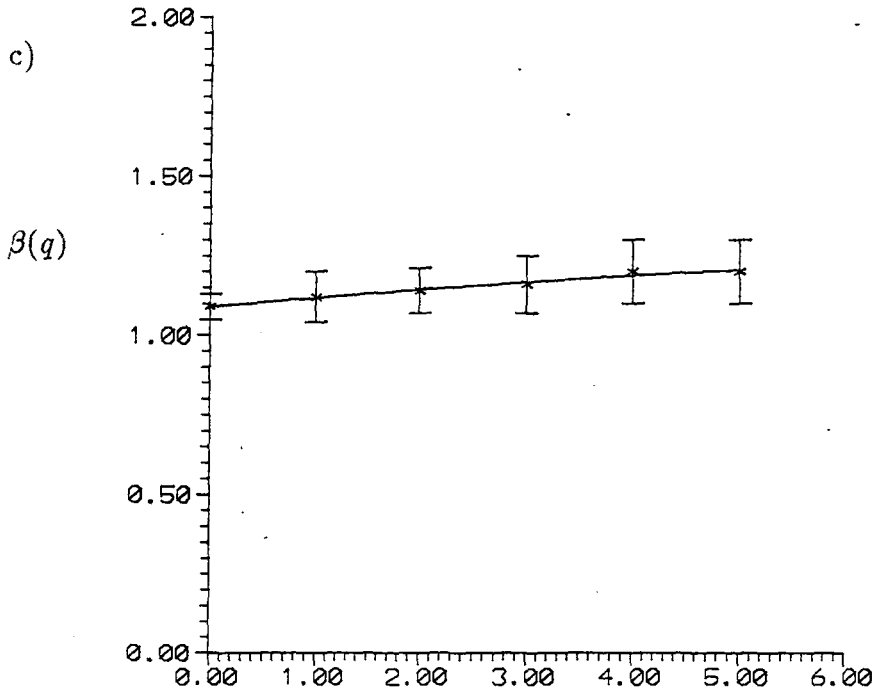

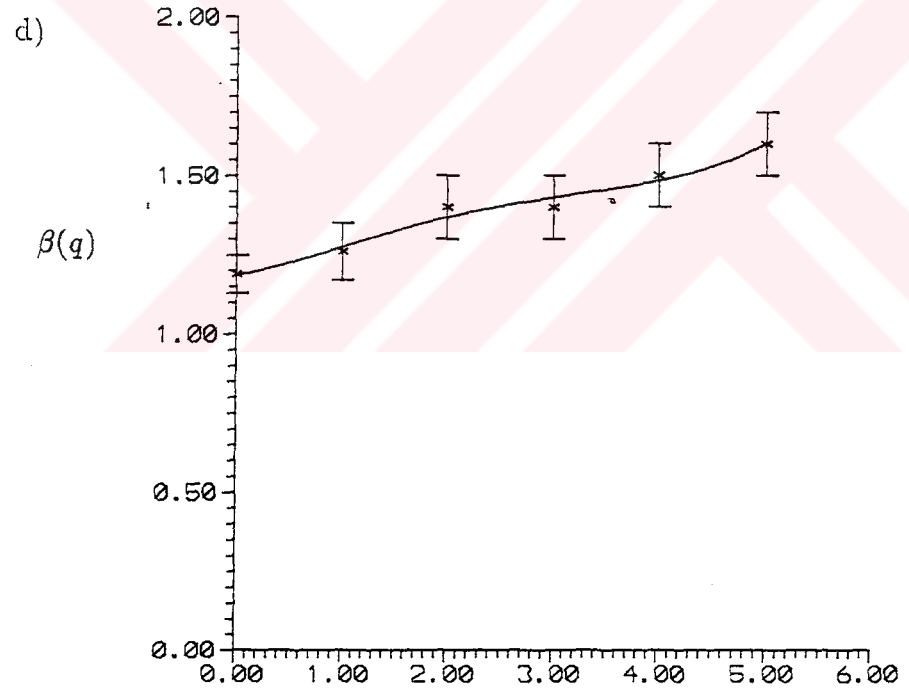

Fig. (2.8) $\beta(q)$ vs.q for the modified tent map, a)$r = 2.539$, $\varepsilon = 0.1$, b)$r = 3$, $\varepsilon = 0.3593$, c)$r = 3.735$, $\varepsilon = 0.7$ d)$r = 3$, $\varepsilon = 0.9083$ (continued).

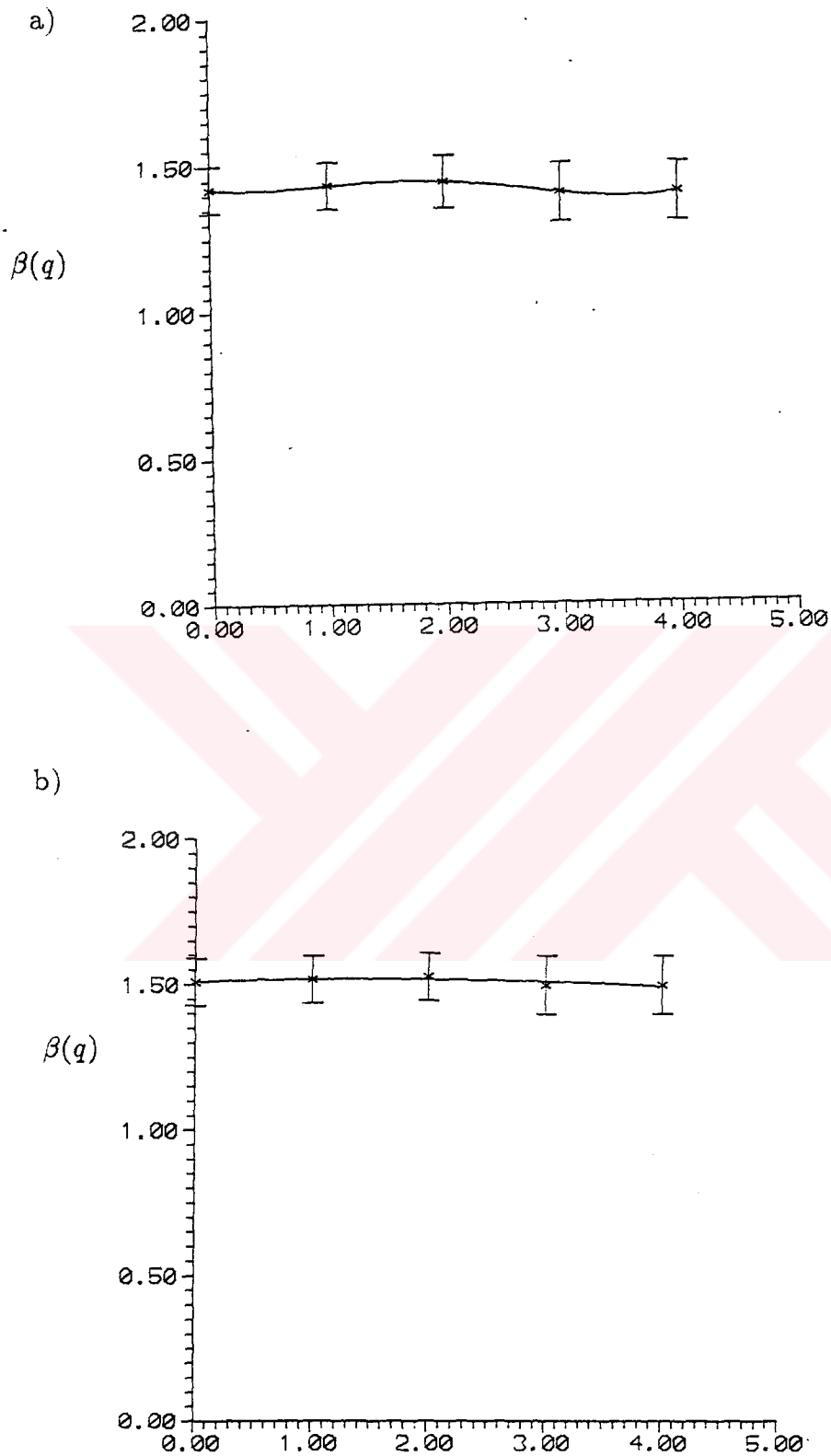

Fig. 2.9 $\beta(q)$ vs. q for the logistic map: a)$\lambda = 3.71$, b)$\lambda = 3.76$, c)$\lambda = 3.81$, d)$\lambda = 3.94$.

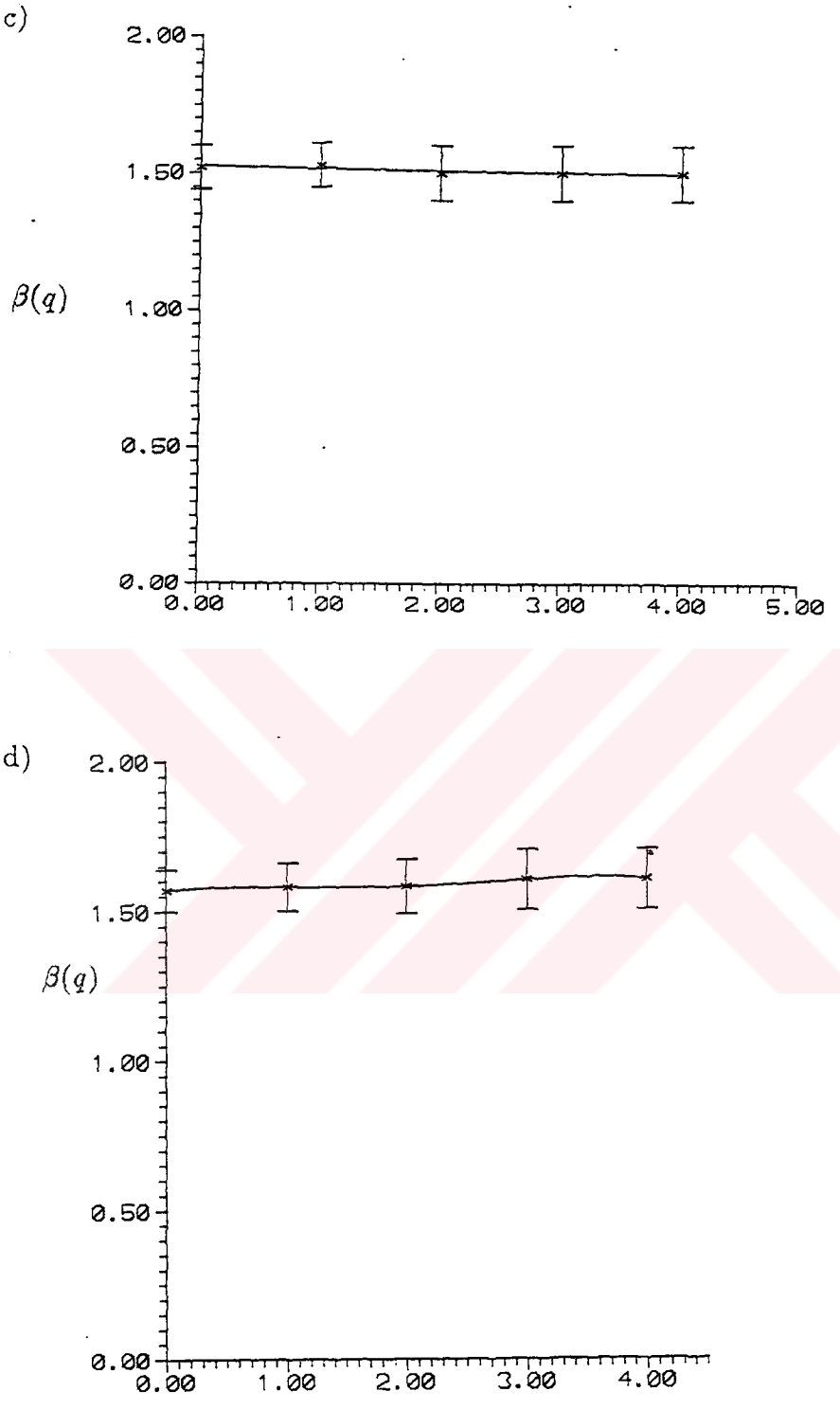

Fig. 2.9 $\beta(q)$ vs. q for the logistic map: a)$\lambda = 3.71$, b)$\lambda = 3.76$, c)$\lambda = 3.81$, d)$\lambda = 3.94$ (continued).

CHAPTER 3. THE STRUCTURE FUNCTIONS

3.1. The Structure Function

The structure functions of the fields are given by,

$$S^q(r) = \left\langle \mid \vec{u}(\vec{x} + \vec{r_0}) - \vec{u}(\vec{x}) \mid^q \right\rangle \tag{3.1}$$

and they are believed to scale as

$$S^q(r) = \lim_{r \to 0} \left\langle \mid \vec{u}(\vec{x} + \vec{r}) - \vec{u}(\vec{x}) \mid^q \right\rangle \sim r^{q\zeta_q} \tag{3.2}$$

where $\vec{u}(\vec{x})$ is the field at point $\vec{x}$, and the average is taken over time and all space.

Although, in the system we use, space is discrete, and the limit $r \to 0$ cannot be taken, we investigate if there is a scaling behavior for some discrete ℓ values ($r_0 \ll \ell \ll L$, where L is the scale on which the possible variations in x_n are registered). The set of dynamical variables x_n can be considered as a one–dimensional field over a discrete space, so the structure functions of the CML can be defined as the differences, S_ℓ, of the fields at two lattice points separated by a distance ℓ ($\ell \ll L$), the lattice spacing being taken as unity:

$$S_\ell = \left\langle \frac{1}{N_\ell} \sum_i^{N_\ell} \mid x_{i+\ell} - x_i \mid \right\rangle. \tag{3.3}$$

where N_ℓ is the number of intervals sized ℓ within the region L, and $< \cdots >$ represents averaging over different time snapshots and different L placements. We expect the first order structure function to scale as

$$S_\ell \sim \left(\frac{\ell}{L}\right)^{\zeta_1}, \tag{3.4}$$

3.2. The Relation Between $\beta(1)$ and ζ_1

Let us consider an interval of size ℓ and look at the piece of graph above it. By taking d–dimensional boxes with linear size (ℓ/L) above the interval, it is seen that the piece of graph above the interval can be covered by $|x_{i+1} - x_i|/(\ell/L)$ boxes of size (ℓ/L) (Fig (3.1)). The number of boxes necessary to cover the interval L is,then,

$$N = \left(\frac{L}{\ell}\right)^d \frac{|x_{i+\ell} - x_i|}{(\ell/L)} \tag{3.5}$$

with d being the dimension of the space.

The average graph length scales as $(\ell/L)^{-\beta(1)}$ as given in Eq. (2.7), and this quantity should be equal to or greater than the average number of boxes necessary to cover the graph.

$$\left(\frac{\ell}{L}\right)^{-\beta(1)} \geq \left(\frac{\ell}{L}\right)^{d+1} \langle\, |x_{i+\ell} - x_i| \,\rangle \tag{3.6}$$

where $< \cdots >$ has the same meaning as before. Using Eq. (3.3), we get,

$$\left(\frac{\ell}{L}\right)^{-\beta(1)} \geq \left(\frac{L}{\ell}\right)^{\zeta_1 - d - 1} \tag{3.7}$$

For this inequality to be true

$$-\beta(1) \geq \zeta_1 - d - 1 \tag{3.8}$$

or

$$\beta(1) \leq d + 1 - \zeta_1 \tag{3.9}$$

This result is a well–known inequality [20]. In our system, $d = 1$, so

$$\beta(1) \leq 2 - \zeta_1 \tag{3.10}$$

It is seen that if the graph tends to be space–filling, $\beta(1)$ will go to 2, and $\zeta_1 \to 0$. On the other hand, if the graph is smooth, $\beta(1)$ will be

1, and therefore $\zeta_1 = 0$. So, the structure function exponent, ζ_1, shows how smoothly or roughly the field varies from point to point.

3.3. q^{th} Order Structure Functions and Their Relation with Generalized Graph Dimensions

Having computed the first order structure function and its relation with the fractal dimension of the graph, one may wonder if there exists such a relation between the q^{th} order structure functions and the generalized graph dimensions. The q^{th} order structure functions are given by

$$S_\ell^q = \left\langle \frac{1}{N_\ell} \sum_{i-1}^{N_\ell} |x_{i+\ell} - x_i|^q \right\rangle \sim \left(\frac{\ell}{L}\right)^{q\zeta_q} \tag{3.11}$$

where $< \cdots >$ has the same meaning as before and $N_\ell = L/\ell$.

The q^{th} moment of the average graph length scales as $(\ell/L)^{-q\beta(q)}$ (Eq. (2.9)), and this quantity should be equal to or greater than the moments of the average number of boxes of size (ℓ/L) needed to cover the part of the graph over an ℓ– sized interval. (We are going to follow the argument used in Section 3.2.)

$$\left(\frac{\ell}{L}\right)^{-q\beta(q)} \geq \left(\frac{L}{\ell}\right)^{q(d+1)} \left\langle |x_{i+\ell} - x_i|^q \right\rangle \tag{3.12}$$

Using Eq. (3.11),

$$\left(\frac{\ell}{L}\right)^{-q\beta(q)} \geq \left(\frac{L}{\ell}\right)^{q(\zeta_q - d - 1)} \tag{3.13}$$

Again for this inequality to be true,

$$-q\beta(q) \geq q(\zeta_q - d - 1) \tag{3.14}$$

or

$$\beta(q) \leq d + 1 - \zeta_q \tag{3.15}$$

In our one–dimensional system, the inequality becomes

$$\beta(q) \leq 2 - \zeta_q \tag{3.16}$$

The ζ_q values we have found for the coupled modified logistic map are shown in Table (3.1), and the scaling of the structure functions are given in Fig (3.1) for different ε_c and r values. In the coupled logistic map, there exists a scaling behavior like for the tent map for some λ values, while there is none for others. This scaling behavior and the breakdown of scaling is shown in Fig. (3.2). When the results in Table (2.2) and Table (3.1) are placed in Eq. (3.14), we see that, even though this inequality is satisfied, it is not saturated.

Table 3.1. $\zeta(q)$ values for different ε_c and r values in the modified tent map.

ζ_q	$\varepsilon_c = .1$ $r = 2.539$	$\varepsilon_c = .3591$ $r = 3$	$\varepsilon_c = .7$ $r = 3.735$	$\varepsilon_c = .9083$ $r = 3$
ζ_1	.13±.05	.11±.04	.13±.05	.15±.06
ζ_2	.09±.05	.08±.07	.08±.05	.0.9±..06
ζ_3	.05±.04	.06±.05	.04±..03	.05±.04

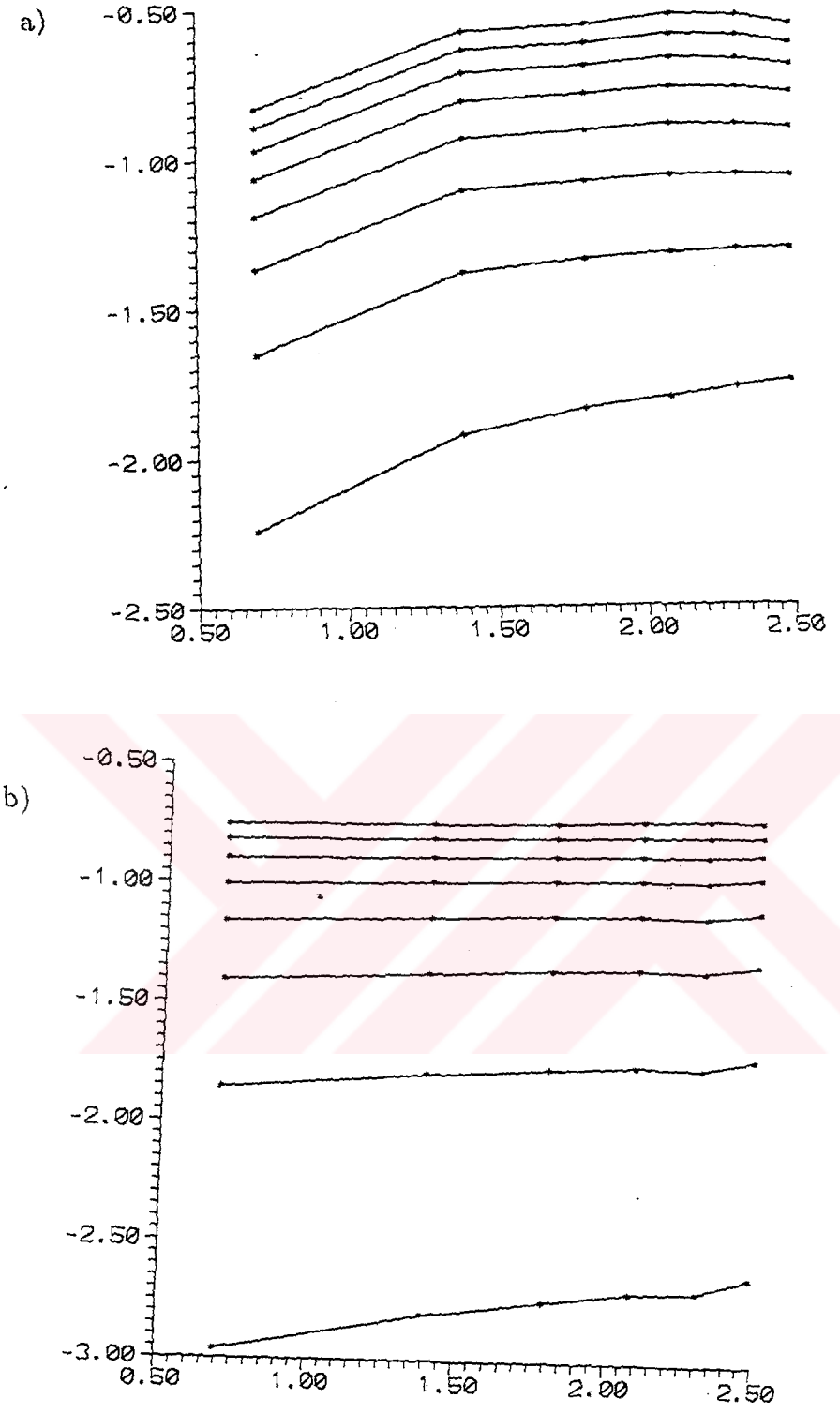

Fig. 3.1. The scaling of the q^{th} order structure functions for different r and ε_c parameters in the modified tent map: a)$r = 2.539$, $\varepsilon_c = 0.1$, b)$r = 3$, $\varepsilon_c = 0.3593$, c)$r = 3.735$, $\varepsilon_c = 0.7$, d)$r = 3$, $\varepsilon_c = 0.9983$.

c)

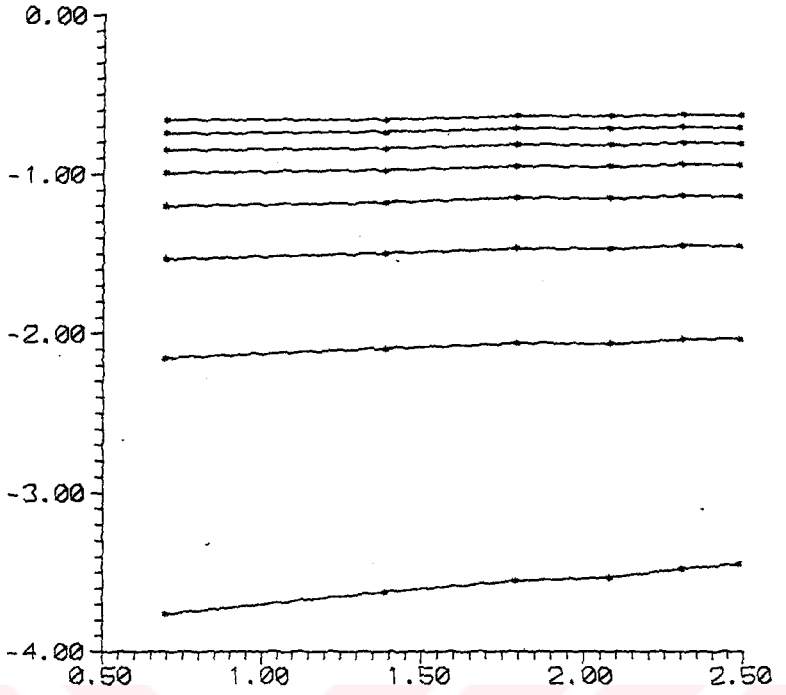

d)

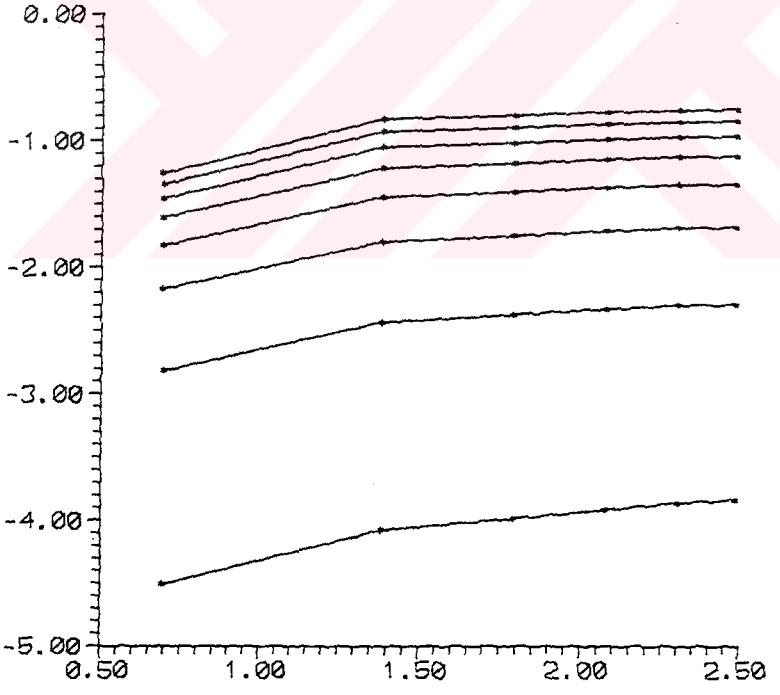

Fig. 3.1. The scaling of the q^{th} order structure functions for different r and ε_c parameters in the modified tent map: a)$r = 2.539$, $\varepsilon_c = 0.1$, b)$r = 3$, $\varepsilon_c = 0.3593$, c)$r = 3.735$, $\varepsilon_c = 0.7$, d)$r = 3$, $\varepsilon_c = 0.9983$ (continued).

a)

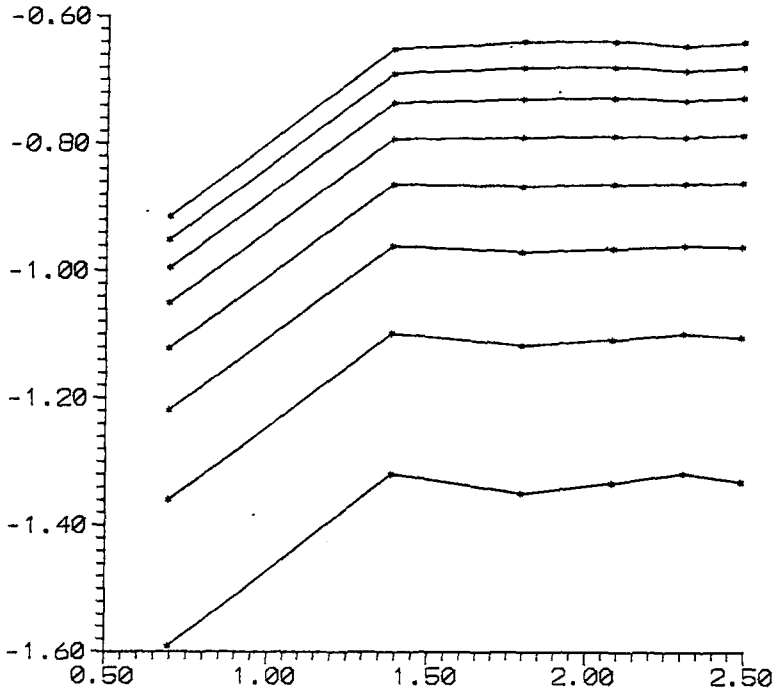

b)

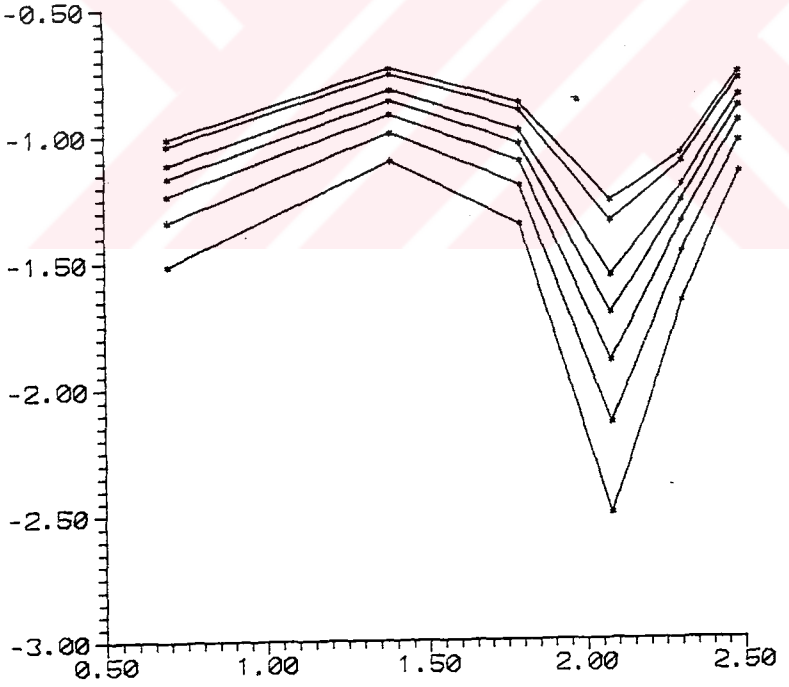

Fig. 3.2 a) The scaling of the q^{th} order structure functions for $\lambda = 3.94$ in the logistic map. b) The breakdown of scaling for $\lambda = 3.76$.

CHAPTER 4. GENERALIZED DIMENSIONS OF THE GRAPH

4.1. Generalized Dimensions

In Chapter 2, it has been shown that the generalized graph dimensions, $\beta(q)$, have a nonlinear dependence on the moments, q, and therefore the wrinkledness of the graph of the CML is not uniformly distributed. We would now like to investigate how this nonlinearity is distributed, so we define a conserved measure.

$$\mu_i(\ell) = \frac{G_i(\ell)}{G_{tot}} \tag{4.1}$$

where G_{tot} is the length of the graph in an L– sized interval (L is the typical scale over which the largest possible variations in x_n are registered), and $\sum_i \mu_i = 1$. The partition function, then, is defined by

$$\chi_\ell(q) = \left\langle \sum_i \mu_i^q(\ell) \right\rangle \tag{4.2}$$

where $< \cdots >$ denotes averaging over different times and different L placements. We expect the partition function to scale as

$$\chi_\ell(q) \sim \left(\frac{\ell}{L}\right)^{\tau(q)} \tag{4.3}$$

where $\tau(q) = (q-1)D(q)$, and $D(q)$ is the generalized dimension [2,4,5,6]. For $q = 0$, the partition function reduces to the number of boxes of size ℓ necessary to cover the L– sized interval, so $D(q = 0)$ is the fractal

dimension of the support of the graph. The information dimension, $D(1)$, is the fractal dimension of the set, on which most of the measure μ lives [29], and is given by

$$D(1) = \lim_{q \to 1} \frac{1}{q-1} \frac{\left\langle \sum_i \mu_i^q(\ell) \right\rangle}{\ln \ell / L} \tag{4.4}$$

where $< \cdots >$ denotes averaging over different snapshots and different L placements throughout the whole system size N. When the limit in Eq. (4.4) is taken, we find

$$D(1) = \frac{\left\langle \sum_i \mu_i \ln \mu_i \right\rangle}{\ln (\ell / L)}. \tag{4.5}$$

If all the boxes have the same measure, then the information dimension will be equal to the fractal dimension of the support, $D(0)$.

If the wrinkledness has multiscaling properties, then the scaling exponents of the measure will differ from one interval to another. So, we define a singularity exponent, α, as

$$\mu_i(\ell) = \left(\frac{\ell}{L} \right)^{\alpha_i} \tag{4.6}$$

The singularity exponent, α, is very much like the singularity exponent γ defined in Chapter 2, Section 2.2, with the difference that small α values belong to the intervals over which the measure is very singularly distributed. One can easily see that

$$\begin{aligned} \chi_\ell(q) &= \sum_i \mu_i^q(\ell) = \sum_i \left(\frac{\ell}{L} \right)^{\alpha_i q} \\ &\sim \left(\frac{\ell}{L} \right)^{(q-1) D(q)} \end{aligned} \tag{4.7}$$

So, when q is increased, the interval with smaller α values will contribute more to the summation in Eq. (4.7), and smaller $D(q)$ will be obtained.

As for $q < 0$, the contribution will come mostly from bigger α values, which correspond to the more uniform parts of the graph, so $D(q)$ will increase.

We can compute the distribution of the singularity exponents directly from the generalized dimensions. If $N_\alpha(\ell)$ is the number of boxes in which the measure has the singularity exponent α, we can associate a dimension $f(\alpha)$ with this subset S_α,

$$N_\alpha(\ell) \sim \left(\frac{\ell}{L}\right)^{-f(\alpha)} \tag{4.8}$$

Then, the partition function can be written in terms of α and $f(\alpha)$ by dividing the summation $\sum_i \mu_i(\ell)$ into a summation over α and a summation over all the subsets S_α that carry such a singularity:

$$\begin{aligned}\chi_\ell(q) &= \sum_i \mu_i^q(\ell) = \sum_i \left(\frac{\ell}{L}\right)^{\alpha_i q} \\ &= \sum_\alpha \sum_{S_\alpha} \left(\frac{\ell}{L}\right)^{\alpha q} = \sum_\alpha \left(\frac{\ell}{L}\right)^{\alpha q} N_\alpha(\ell) \\ &= \sum_\alpha \left(\frac{\ell}{L}\right)^{\alpha q - f(\alpha)} \sim \int \left(\frac{\ell}{L}\right)^{q\alpha - f(\alpha)} d\alpha\end{aligned} \tag{4.9}$$

For small (ℓ/L), the integral will be dominated by the minimum of the exponents, so if a saddle point approximation is made, using Eq. (4.3), we get

$$\tau(q) = q\alpha(q) - f(\alpha(q)), \tag{4.10.a}$$

$$\frac{\partial f(\alpha(q))}{\partial \alpha} = q, \tag{4.10.b}$$

$$\frac{\partial \tau(q)}{\partial q} = \alpha(q). \tag{4.10.c}$$

This is a Legendre transformation from the function $\tau(q)$ to $f(\alpha)$. If we know the generalized dimensions, $D(q)$, we can find the $f(\alpha)$ spectrum by performing this Legendre transformation.

The numerical results for $D(q)$ values for parameters are given in Table (4.1), and the scaling of $\chi_\ell(q)$ for different parameters are shown in Figs. (4.1) and (4.2) for the modified tent map and the logistic map, respectively. We have seen that, for the tent map, in the turbulent region, $\chi_\ell(q)$ has no scaling behavior (Fig. (4.3.a)). On the other hand, in the laminar region $D(q) = D(0) = 1$ (Fig. (4.3.b)). The graphs of $D(q)$ vs q and the $f(\alpha)$ spectra are shown in Figs. (4.4)–(4.5) and (4.6)–(4.7), respectively (The first figures belong to the modified tent map, the latter to the logistic map).

4.2. The Relation Between $D(q)$ and $\beta(q)$

In Chapter 2, the moments of the average graph length, $\langle G_\ell \rangle$ has been given by Eq. (2.8). Taking $q = 1$ in this equation, we can find the total graph length in an interval of size L, G_{tot},

$$\begin{aligned} G_{tot} &= \left(\frac{L}{\ell}\right)^d \langle G_\ell \rangle \\ &= \left(\frac{L}{\ell}\right)^d \left(\frac{\ell}{L}\right)^{-\beta(1)} \\ &= \left(\frac{\ell}{L}\right)^{-d-\beta(1)} \end{aligned} \tag{4.11}$$

where d is the dimension of the space. So, the conserved measure $\mu_i(\ell)$ can be rewritten as

$$\begin{aligned} \mu_i(\ell) &= \frac{G_i(\ell)}{G_{tot}} \leq \frac{(\ell/L)^{-\gamma_i}}{(\ell/L)^{-d-\beta(1)}} \\ &\leq \left(\frac{\ell}{L}\right)^{d+\beta(1)-\gamma_i} \end{aligned} \tag{4.12}$$

If we rewrite the generalized dimensions,

$$\begin{aligned} \left(\frac{\ell}{L}\right)^{(q-1)D(q)} &\sim \left\langle \sum_i \mu_i^q(\ell) \right\rangle \\ &\leq \left\langle \sum_{i=1}^{N_\ell} \left(\frac{\ell}{L}\right)^{[d+\beta(1)-\gamma_i]q} \right\rangle \end{aligned} \tag{4.13}$$

The quantity $(\ell/L)^{[d+\beta(1)]q}$ can be taken out of the average, so Eq. (4.13) can be written as

$$\left(\frac{\ell}{L}\right)^{(q-1)D(q)} \leq \left(\frac{\ell}{L}\right)^{[d+\beta(1)]q} \left\langle \sum_{i=1}^{N_\ell} \left(\frac{\ell}{L}\right)^{-\gamma_i q} \right\rangle \tag{4.14}$$

Remembering Eq. (2.9), we see that

$$\begin{aligned} \left\langle \left(\frac{\ell}{L}\right)^{-\gamma_i q} \right\rangle &\sim N_\ell \left(\frac{\ell}{L}\right)^{-q\beta(q)} \\ &= \left(\frac{L}{\ell}\right)^{d} \left(\frac{\ell}{L}\right)^{-q\beta(q)} \\ &= \left(\frac{\ell}{L}\right)^{-d-q\beta(q)} \end{aligned} \tag{4.15}$$

If we put Eq. (4.15) into Eq.(4.14), we find

$$\left(\frac{\ell}{L}\right)^{(q-1)D(q)} \leq \left(\frac{\ell}{L}\right)^{[d+\beta(1)]q-[d+q\beta(q)]} \tag{4.16}$$

So,

$$\begin{aligned} D(q) &\leq \frac{1}{q-1}\{[d+\beta(1)]q - [d+q\beta(q)]\} \\ &\leq \frac{q}{q-1}[\beta(1) - \beta(q)] + d \end{aligned} \tag{4.17}$$

Since, in our system, $d = 1$, we find

$$D(q) \leq \frac{q}{q-1}[\beta(1) - \beta(q)] + 1 \tag{4.18}$$

When we put the results shown in Tables (2.2) and (4.1) into this inequality for the coupled modified tent map, we see that the inequality is numerically verified. The results of the coupled logistic map (Tables (2.3) and (4.2)) also satisfy this relation.

If we replace Eq. (3.14) in Eq. (4.18), we see that

$$D(q) \leq \frac{q}{q-1}(\zeta_q - \zeta_1) + 1 \tag{4.19}$$

When we put the numerical results of Tables (3.1) and (4.1) into Eq. (4.19), it is seen that this inequality is satisfied, but not saturated.

Table 4.1. $D(q)$ values for different ε_c and r values in the modified tent map.

$D(q)$	$\varepsilon_c = .1$ $r = 2.539$	$\varepsilon_c = .3591$ $r = 3$	$\varepsilon_c = .7$ $r = 3.735$	$\varepsilon_c = .9083$ $r = 3$
$D(-4)$	1.3±.1	1.13±.09	1.03±.02	1.2±.1
$D(-3)$	1.2±.1	1.09±.06	1.02±.03	1.1±.06
$D(-2)$	1.12±.07	1.05±.04	1.02±.02	1.09±.06
$D(-1)$	1.05±.03	1.03±.02	1.01±.01	1.04±.02
$D(0)$	1	1	1	1
$D(1)$	.95±.03	.98±.02	.99±.007	.97±.02
$D(2)$	.89±.07	.97±.03	.98±.02	.93±.04
$D(3)$	.8±.1	.91±.06	.97±.02	.89±.07
$D(4)$	.7±.2	.87±.1	.96±.03	.86±.09
$D(5)$	.7±.2	.8±.1	.95±.05	.8±.1

Table 4.2 $D(q)$ values for different λ parameters in the logistic map.

$D(q)$	$\lambda = 3.71$	$\lambda = 3.76$	$\lambda = 3.81$	$\lambda = 3.94$
$D(-4)$	1.14±.09	1.12±.09	1.16±.09	1.2±.1
$D(-3)$	1.11±.07	1.07±.06	1.12±.07	1.15±.09
$D(-2)$	1.08±.09	1.05±.04	1.08±.05	1.08±.05
$D(-1)$	1.04±.04	1.02±.03	1.04±.02	1.04±.02
$D(0)$	1	1	1	1
$D(1)$	.96±.02	.97±.03	.96±.02	.95±.05
$D(2)$	.93±.04	.94±.05	.93±.04	.92±.05
$D(3)$	.9±.06	.91±.06	.89±.06	.88±.09
$D(4)$	.87±.08	.88±.09	.87±.07	.8±.1
$D(5)$	.85±.08	.8±.1	.84±.08	.8±.1

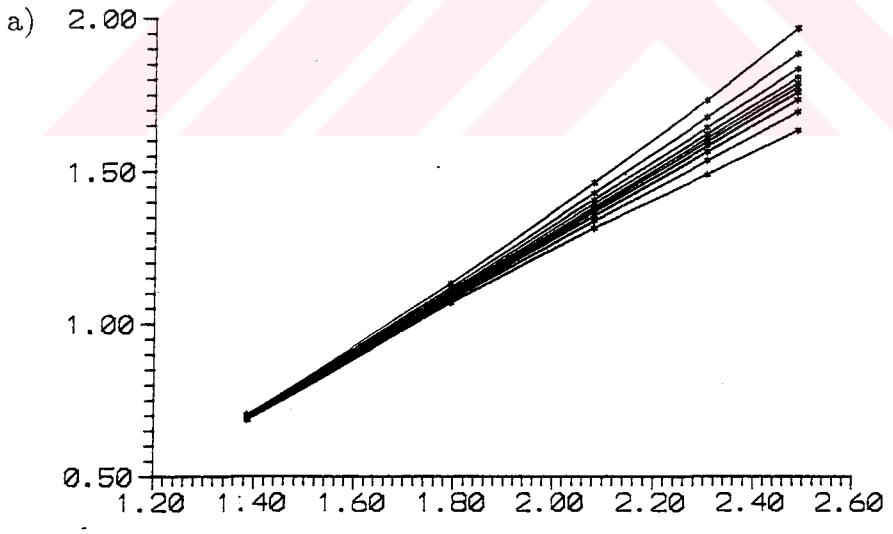

Fig. 4.1. The scaling of the moments of the partition function, $\chi_\ell(q)$, for the coupled modified tent map: a)$r = 2.539$, $\varepsilon_c = 0.1$, b)$r = 3$, $\varepsilon_c = 0.3593$, c)$r = 3.735$, $\varepsilon_c = 0.7$, d)$r = 3$, $\varepsilon_c = 0.9983$.

b)

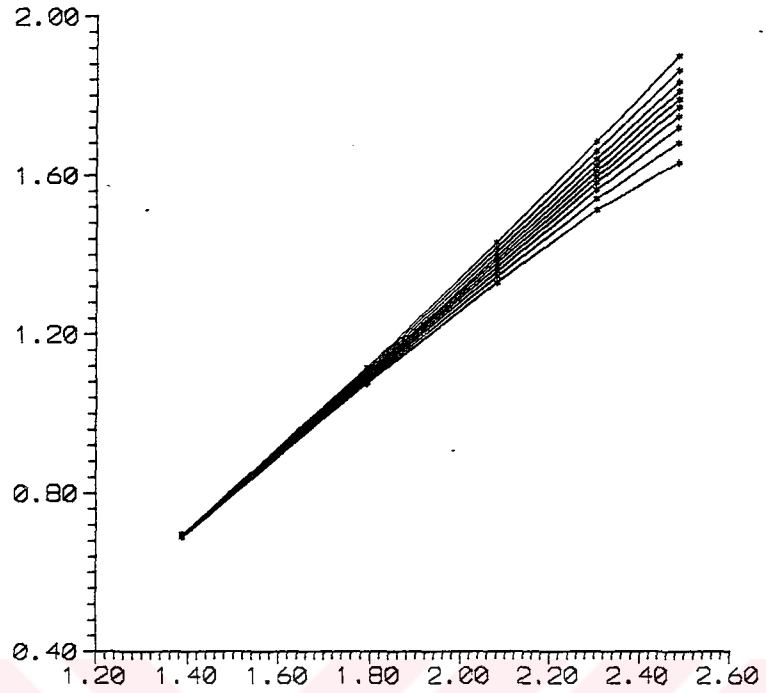

c)

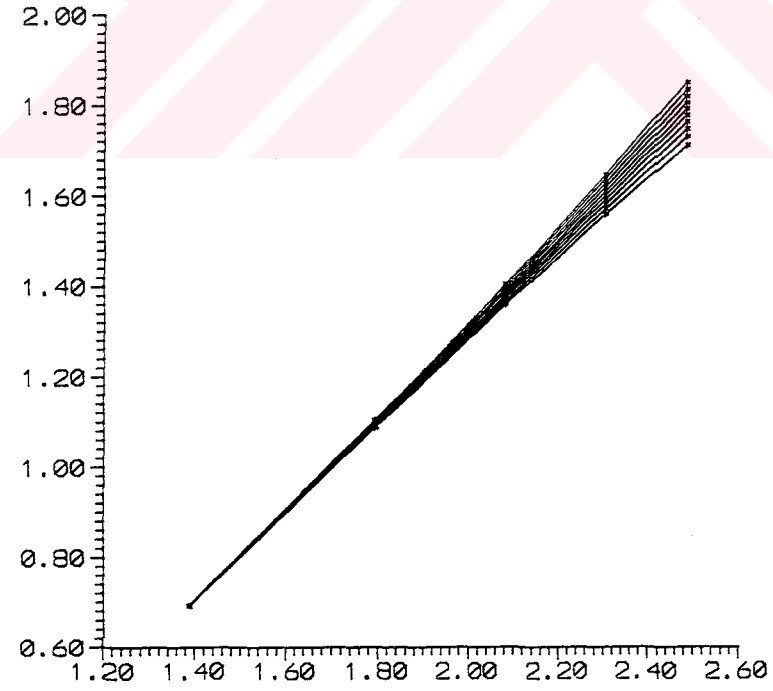

Fig. 4.1. The scaling of the moments of the partition function, $\chi_\ell(q)$, for the coupled modified tent map: a)$r = 2.539$, $\varepsilon_c = 0.1$, b)$r = 3$, $\varepsilon_c = 0.3593$, c)$r = 3.735$, $\varepsilon_c = 0.7$, d)$r = 3$, $\varepsilon_c = 0.9983$ (continued).

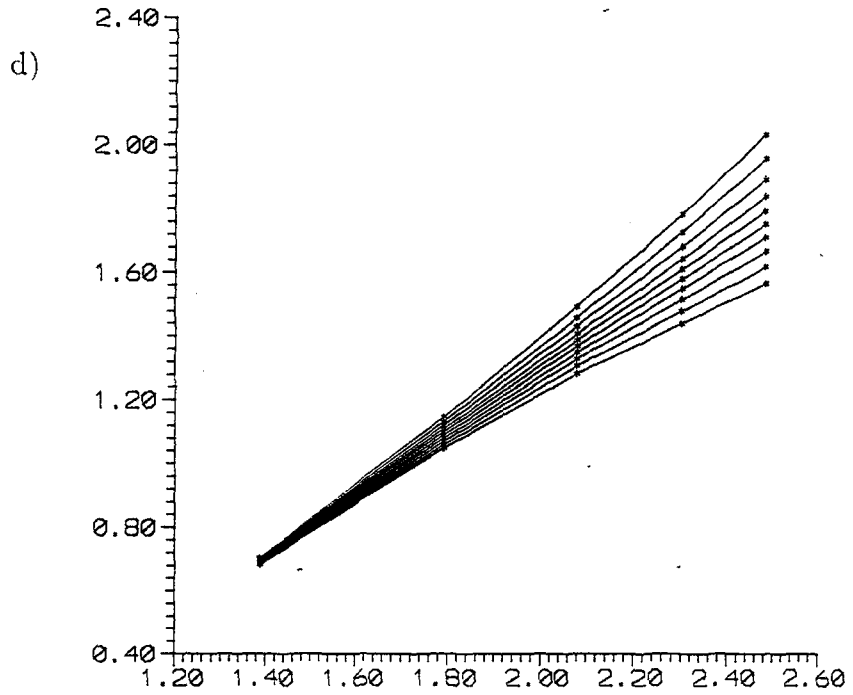

Fig. 4.1. The scaling of the moments of the partition function, $\chi_\ell(q)$, for the coupled modified tent map: a)$r = 2.539$, $\varepsilon_c = 0.1$, b)$r = 3$, $\varepsilon_c = 0.3593$, c)$r = 3.735$, $\varepsilon_c = 0.7$, d)$r = 3$, $\varepsilon_c = 0.9983$ (continued).

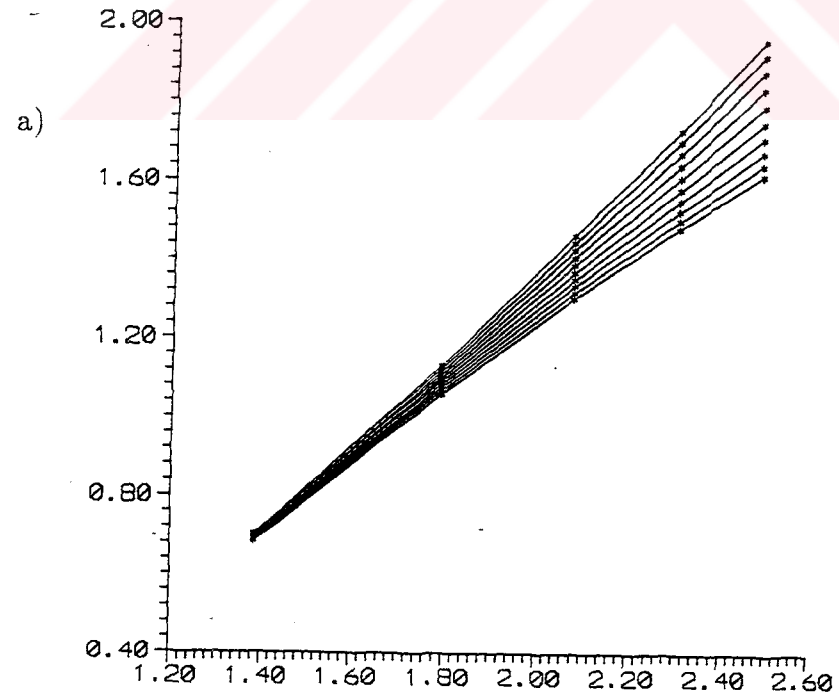

Fig. 4.2 The scaling of the moments of the partition function, $\chi_\ell(q)$, for the coupled logistic map : a)$\lambda = 3.71$, b)$\lambda = 3.76$, c)$\lambda = 3.81$, d)$\lambda = 3.94$.

b)

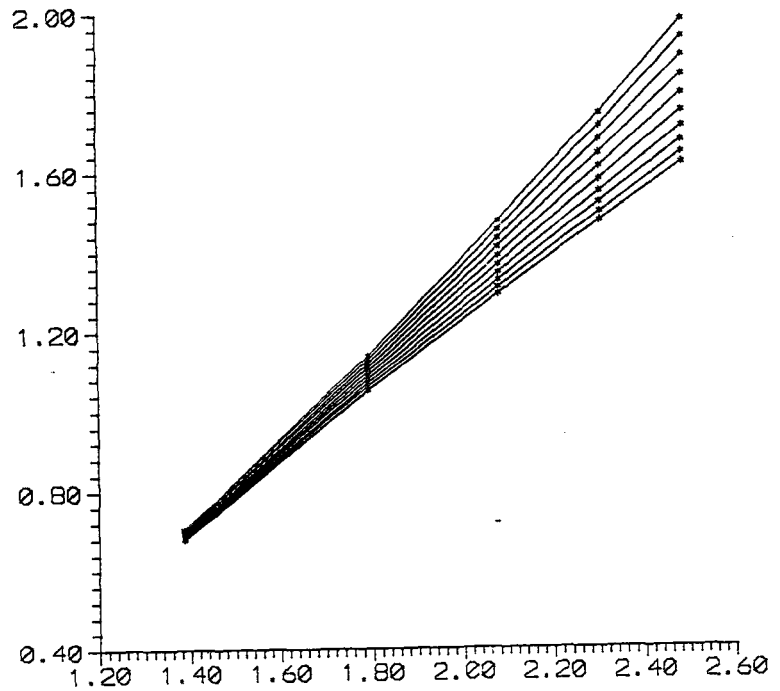

c)

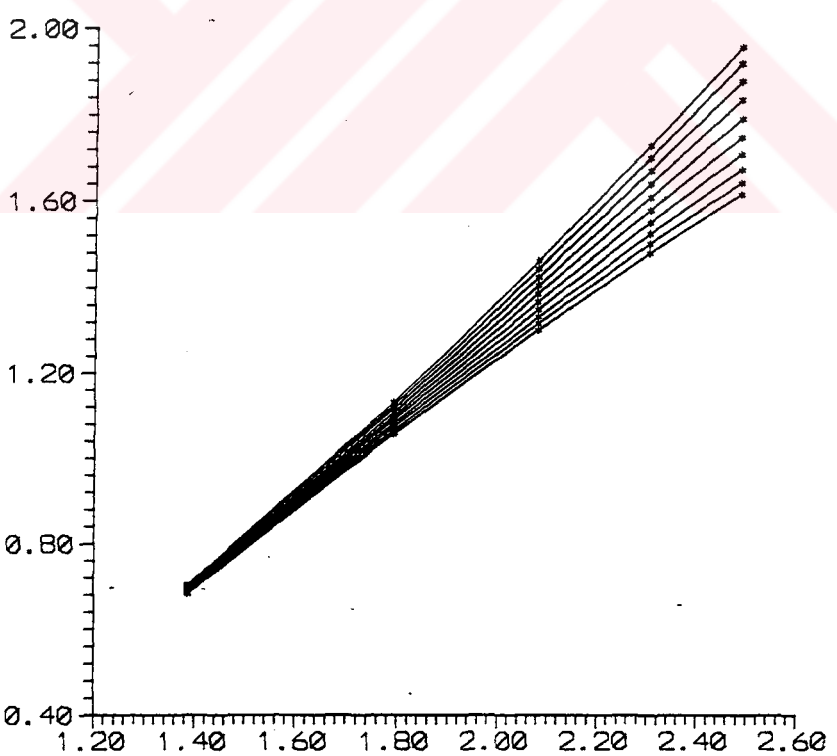

Fig. 4.2 The scaling of the moments of the partition function $\chi_\ell(q)$ for the coupled logistic map: a)$\lambda = 3.71$, b)$\lambda = 3.76$, c)$\lambda = 3.81$, d)$\lambda = 3.94$ (continued).

d)

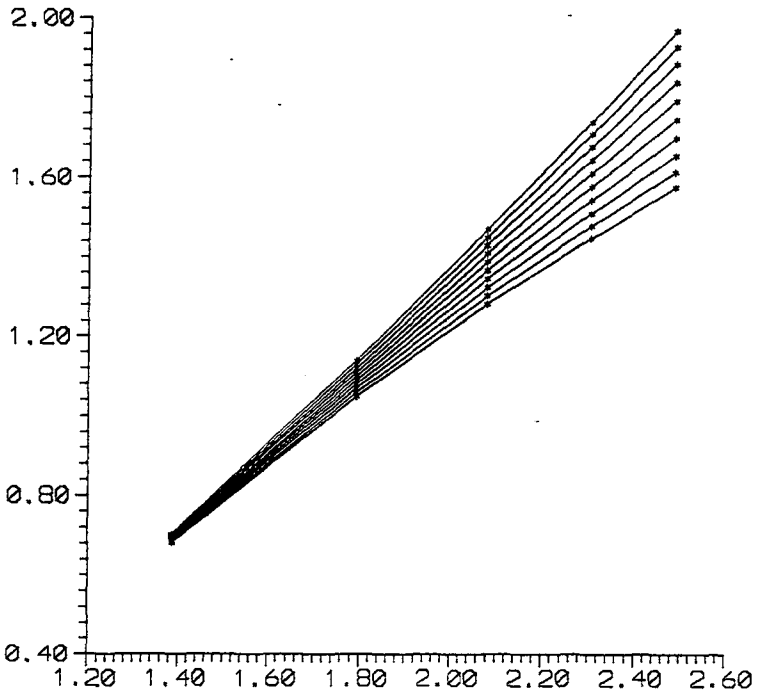

Fig. 4.2 The scaling of the moments of the partition function $\chi_\ell(q)$ for the coupled logistic map: a)$\lambda = 3.71$, b)$\lambda = 3.76$, c)$\lambda = 3.81$, d)$\lambda = 3.94$ (continued).

a)

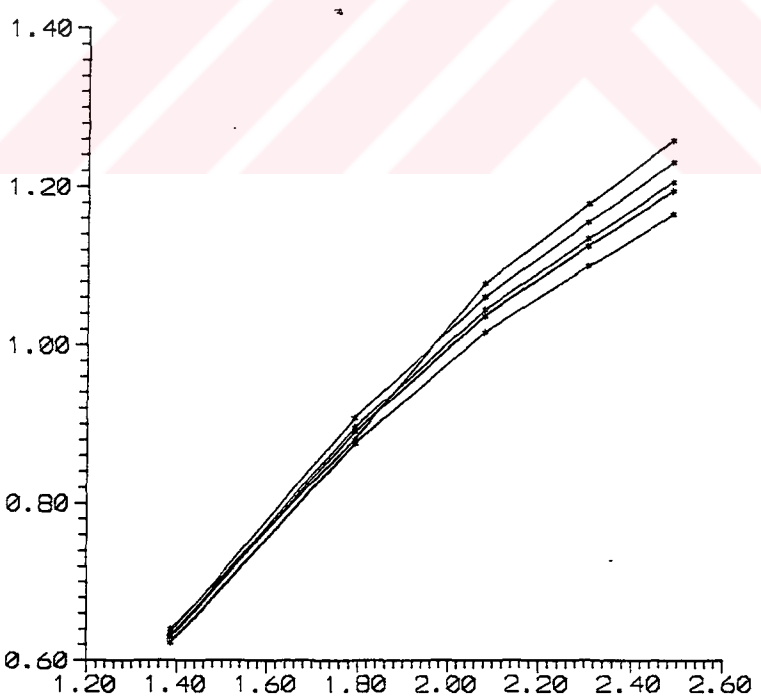

Fig. 4.3 a) The breakdown of scaling the momemts of the partition function, $\chi_\ell(q)$, in the turbulent region for the modified tent map, b) Scaling of the moments of the partition function in the laminar region.

b)

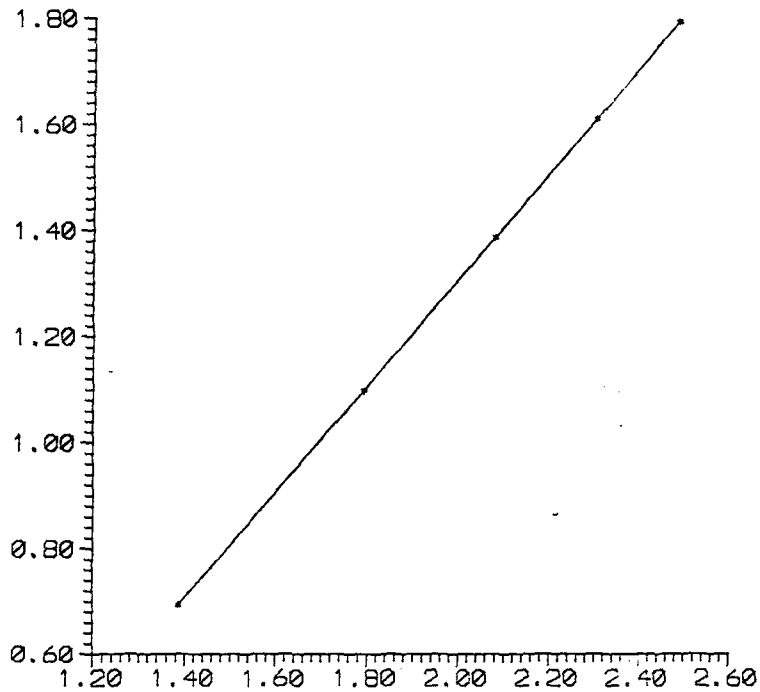

Fig. 4.3 a) The breakdown of scaling the moments of the partition function, $\chi_\ell(q)$, in the turbulent region for the modified tent map, b) Scaling of the moments of the partition function in the laminar region (continued).

a)

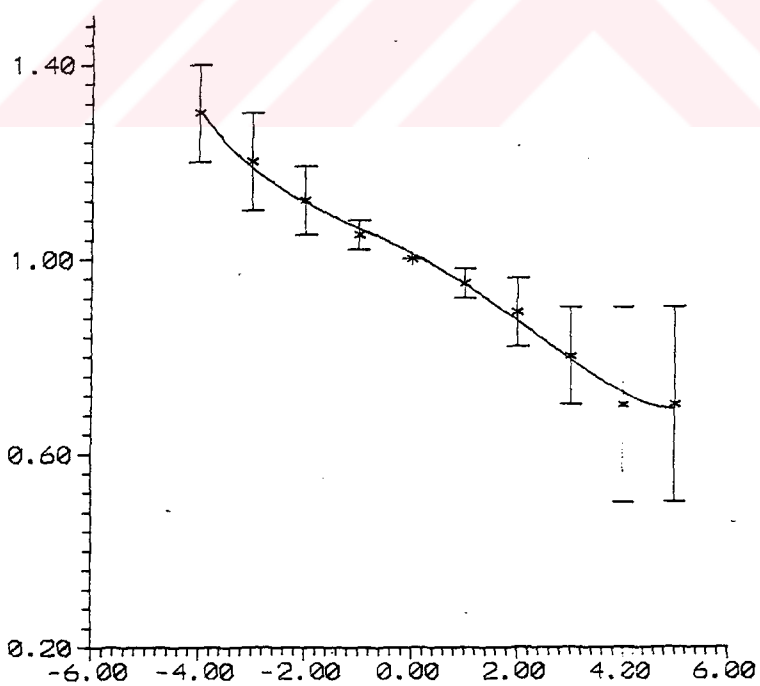

Fig. 4.4. $D(q)$ vs. q for the modified tent map: a)$r = 2.539$, $\varepsilon_c = 0.1$, b)$r = 3$, $\varepsilon_c = 0.3593$, c)$r = 3.735$, $\varepsilon_c = 0.7$, d)$r = 3$, $\varepsilon_c = 0.9983$.

b)

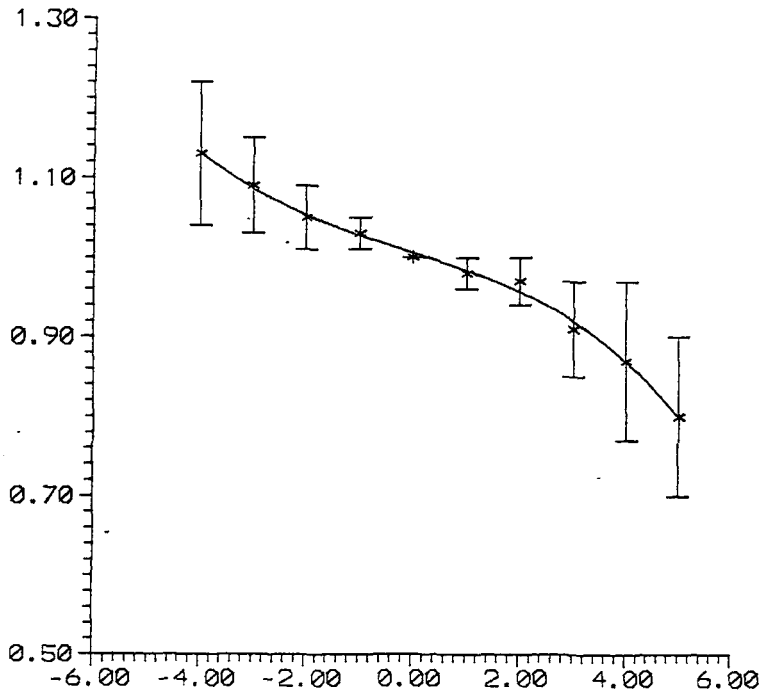

c)

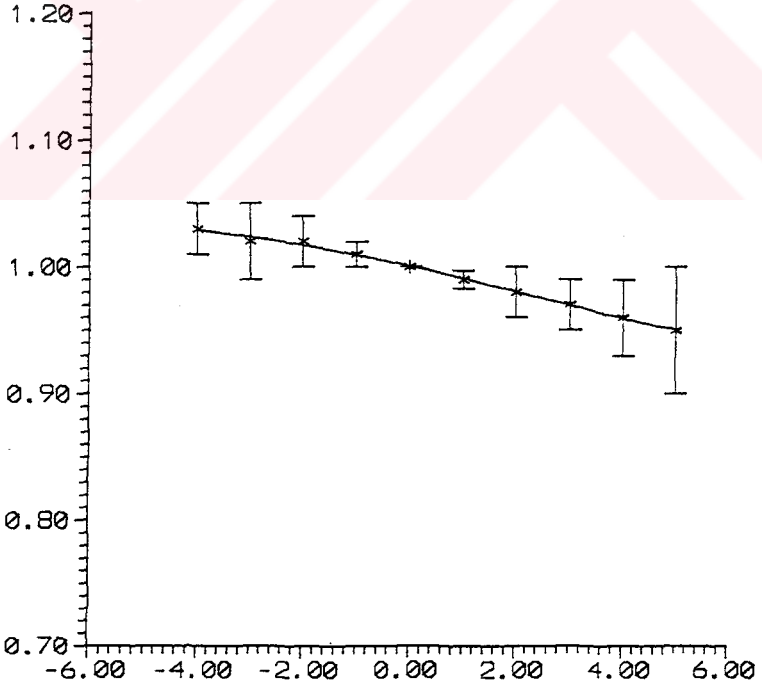

Fig. 4.4. $D(q)$ vs. q for the modified tent map: a)$r = 2.539$, $\varepsilon_c = 0.1$, b)$r = 3$, $\varepsilon_c = 0.3593$, c)$r = 3.735$, $\varepsilon_c = 0.7$, d)$r = 3$, $\varepsilon_c = 0.9983$ (continued).

d)

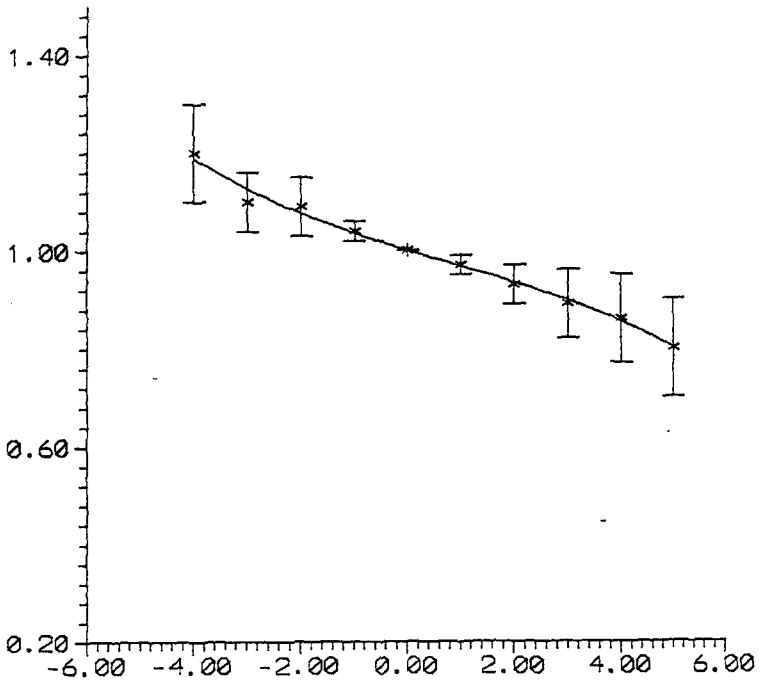

Fig. 4.4. $D(q)$ vs. q for the modified tent map: a)$r = 2.539$. $\varepsilon_c = 0.1$, b)$r = 3$, $\varepsilon_c = 0.3593$, c)$r = 3.735$, $\varepsilon_c = 0.7$, d)$r = 3$. $\varepsilon_c = 0.9983$ (continued).

a)

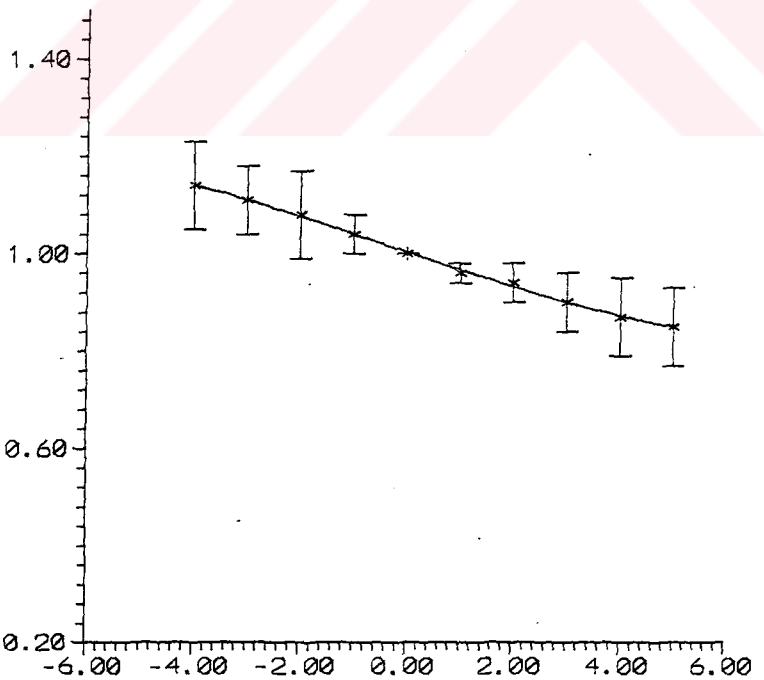

Fig. 4.5 $D(q)$ vs. q for the logistic map: a)$\lambda = 3.71$, b)$\lambda = 3.76$, c)$\lambda = 3.81$, d)$\lambda = 3.94$.

b)

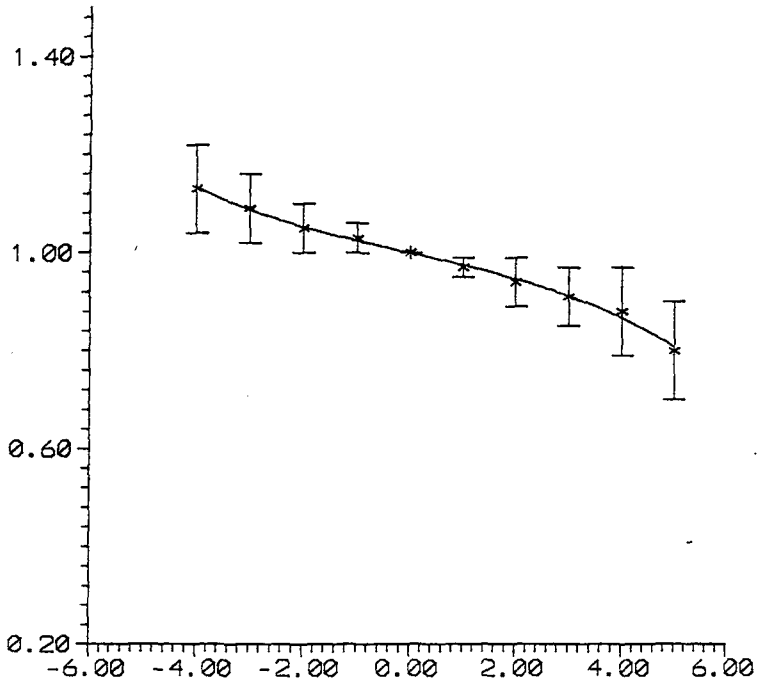

c)

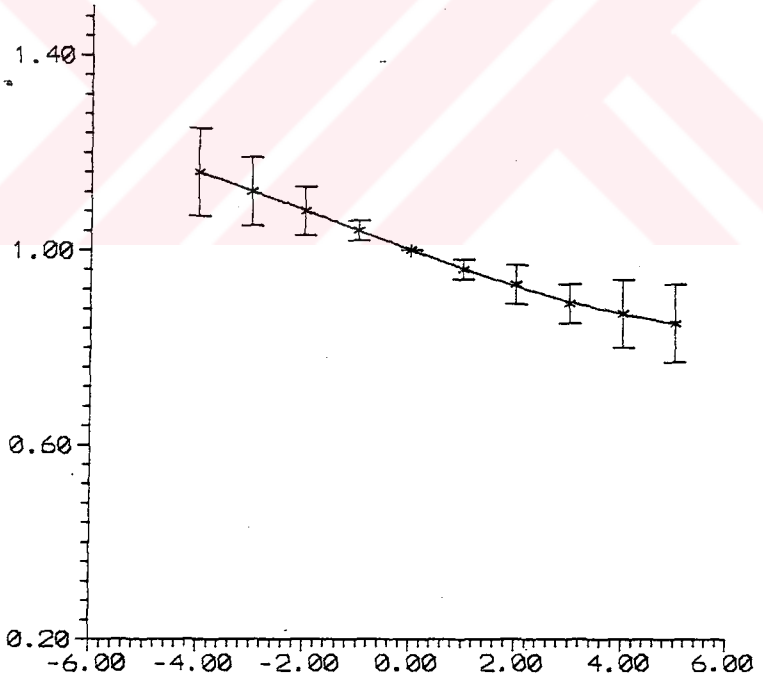

Fig. 4.5 $D(q)$ vs. q for the logistic map: a)$\lambda = 3.71$, b)$\lambda = 3.76$, c)$\lambda = 3.81$, d)$\lambda = 3.94$ (continued).

d)

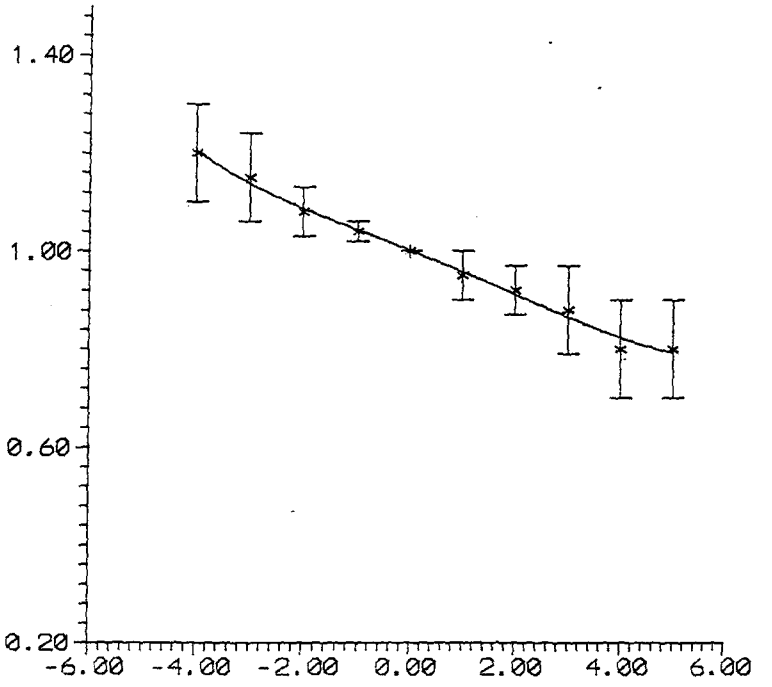

Fig. 4.5 $D(q)$ vs. q for the logistic map: a)$\lambda = 3.71$, b)$\lambda = 3.76$. c)$\lambda = 3.81$, d)$\lambda = 3.94$ (continued).

a)

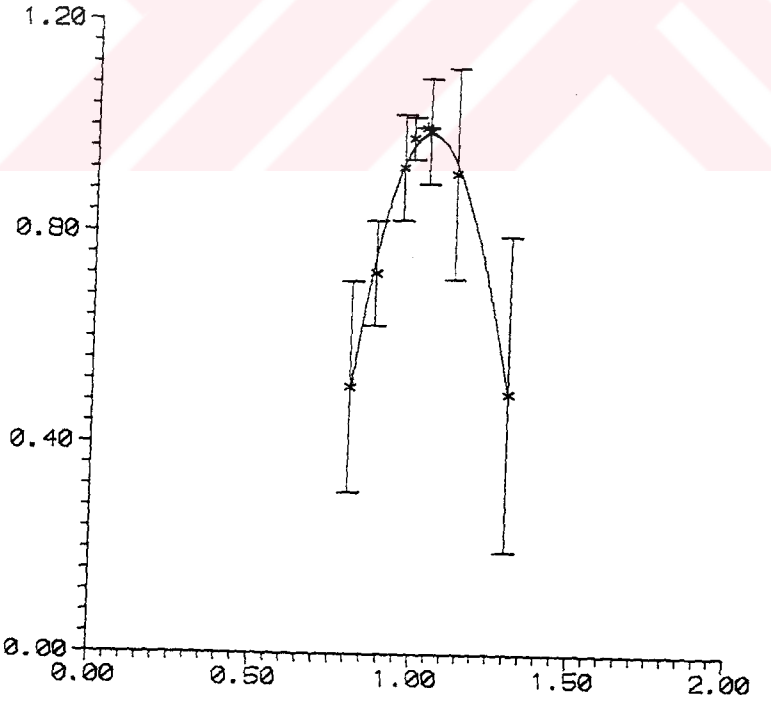

Fig. 4.6. $f(\alpha)$ spectra for the modified tent map: a)$r = 2.539$, $\varepsilon_c = 0.1$, b)$r = 3$, $\varepsilon_c = 0.3593$, c)$r = 3.735$, $\varepsilon_c = 0.7$, d)$r = 3$, $\varepsilon_c = 0.9983$.

b)

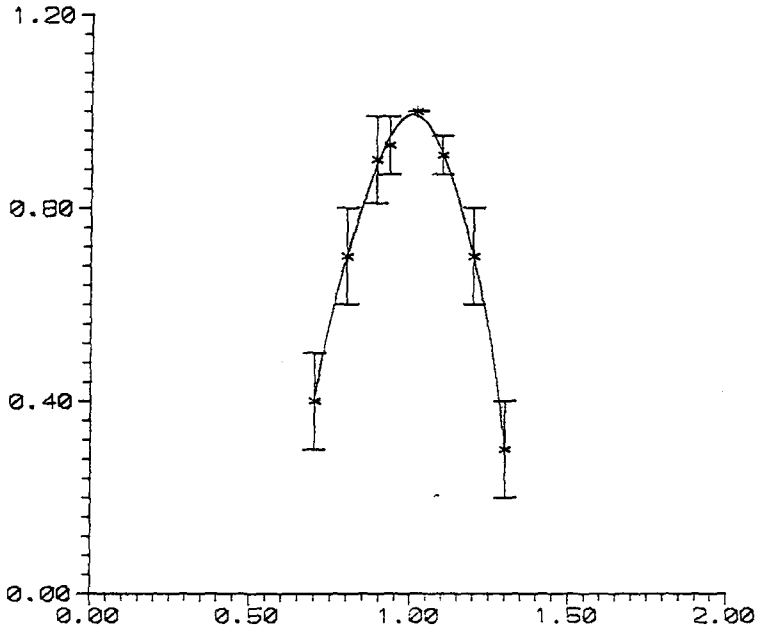

c)

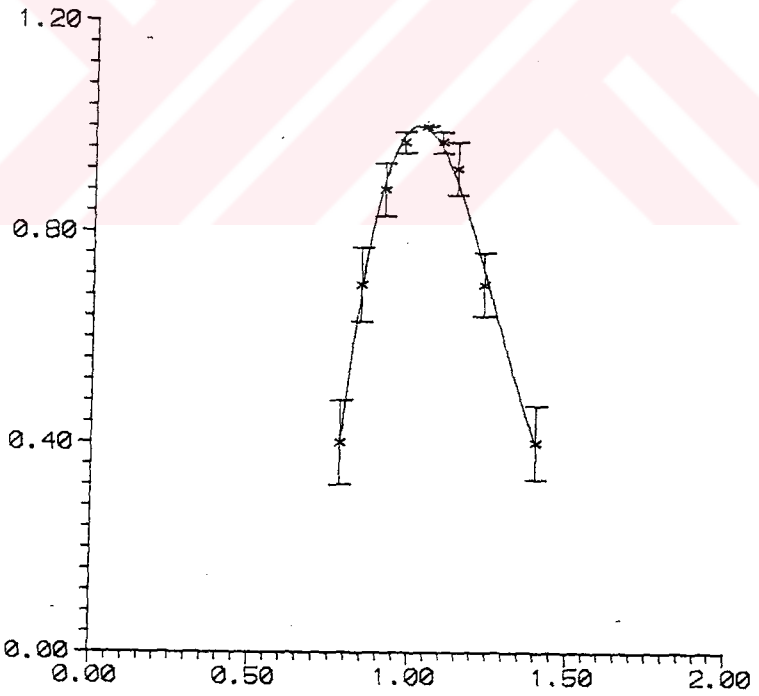

Fig. 4.6. $f(\alpha)$ spectra for the modified tent map: a)$r = 2.539$, $\varepsilon_c = 0.1$, b)$r = 3$, $\varepsilon_c = 0.3593$, c)$r = 3.735$, $\varepsilon_c = 0.7$, d)$r = 3$, $\varepsilon_c = 0.9983$ (continued).

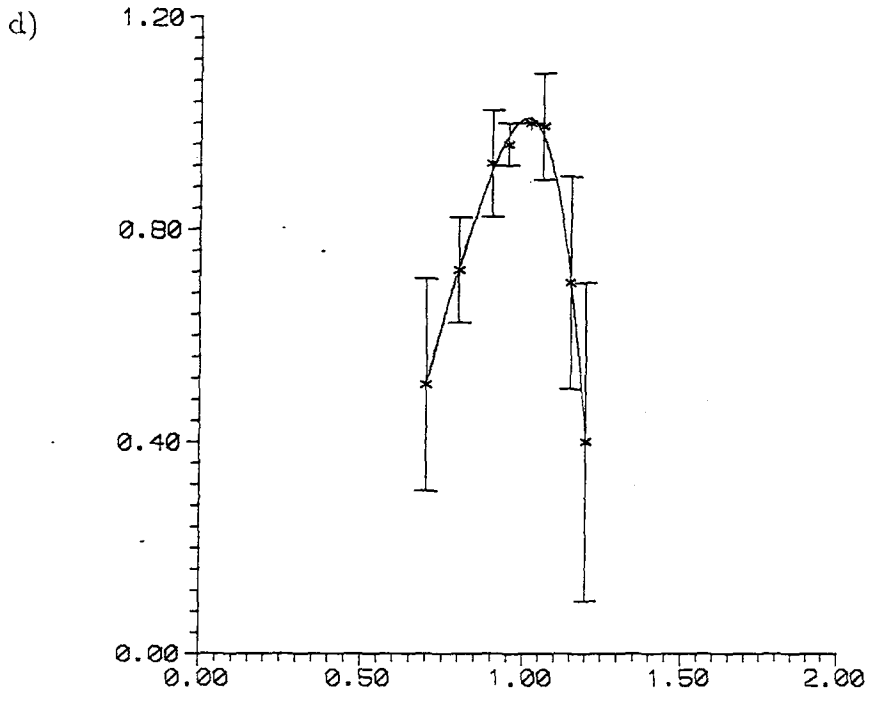

Fig. 4.6. $f(\alpha)$ spectra for the modified tent map: a)$r = 2.539$, $\varepsilon_c = 0.1$, b)$r = 3$, $\varepsilon_c = 0.3593$, c)$r = 3.735$, $\varepsilon_c = 0.7$, d)$r = 3$, $\varepsilon_c = 0.9983$ (continued).

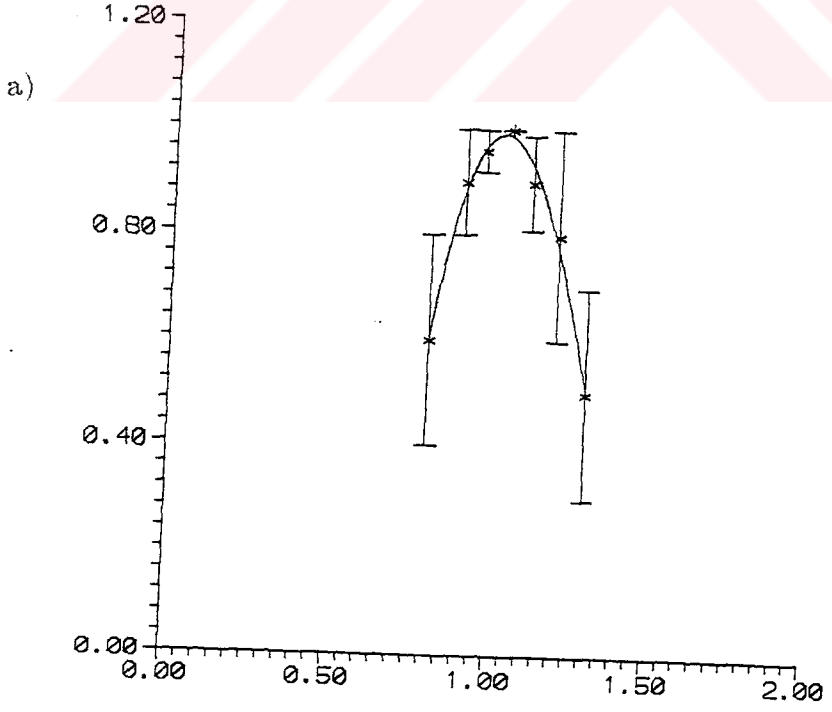

Fig. 4.7 The $f(\alpha)$ spectra for the coupled logistic map : a)$r = 3.71$, b)$r = 3.76$, c)$r = 3.81$, d)$r = 3.94$.

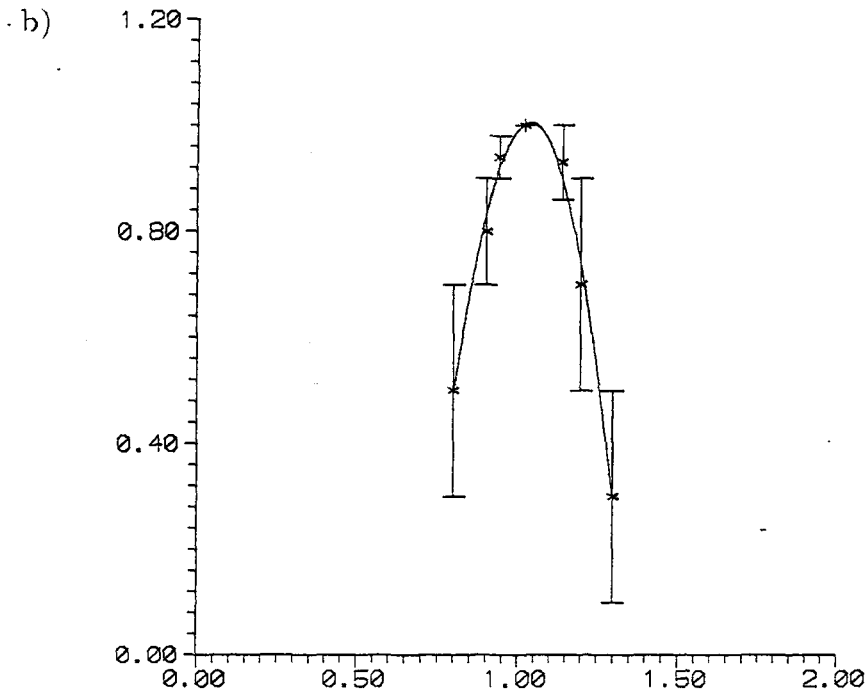

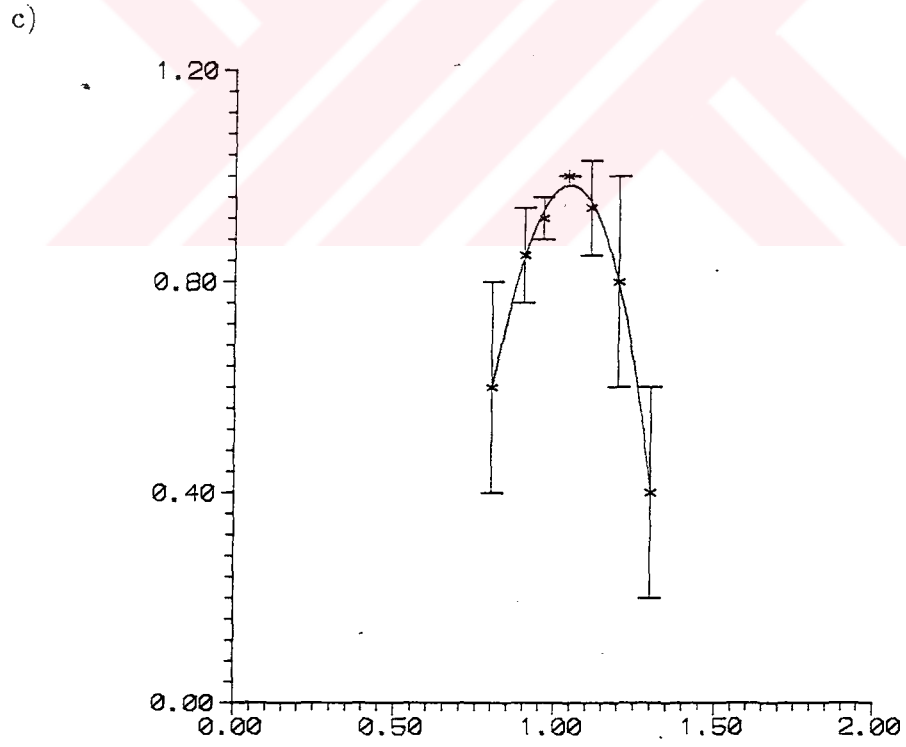

Fig. 4.7 $f(\alpha)$ spectra for the logistic map: a)$\lambda = 3.71$, b)$\lambda = 3.76$, c)$\lambda = 3.81$, d)$\lambda = 3.94$ (continued).

d)

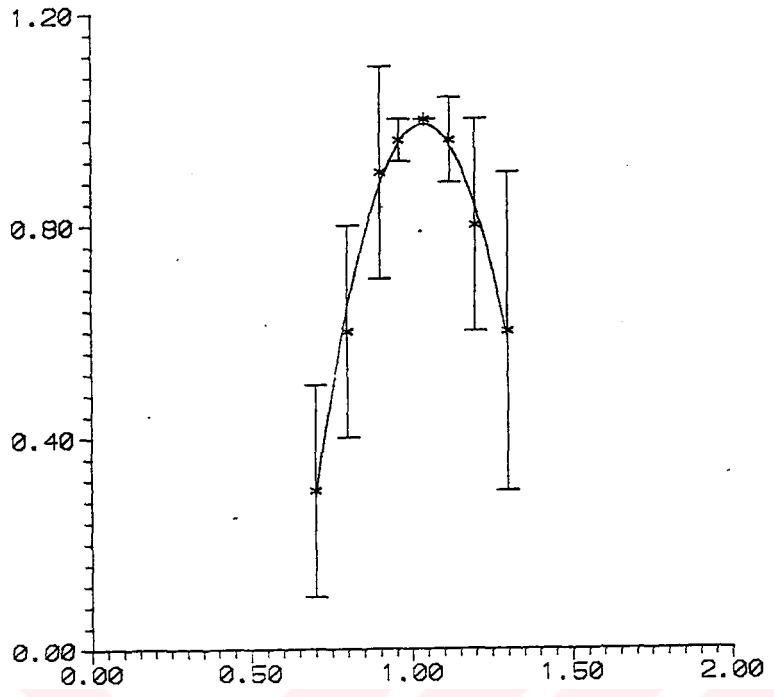

Fig. 4.7 $f(\alpha)$ spectra for the logistic map: a)$\lambda = 3.71$, b)$\lambda = 3.76$, c)$\lambda = 3.81$, d)$\lambda = 3.94$ (continued).

CHAPTER 5. RESULTS

In this study, we have investigated the distribution of wrinkledness of the graph of the CML by means of the generalized graph dimensions and the generalized dimensions of the support of the graph.

We have found from our simulations that the graph length indeed exhibits scaling behavior, as can be seen from the quality of the fits in Figs. (2.6–7). Moreover, we see experimentally that the wrinkledness is not equally distributed. The generalized graph dimensions, $\beta(q)$ were defined as

$$\left(\frac{\ell}{L}\right)^{-q\beta(q)} \sim \left\langle \frac{1}{N_\ell} \sum_i^{N_\ell} G_i^q(\ell) \right\rangle \tag{5.1}$$

where $N_\ell = L/\ell$ is the number of ℓ–sized intervals in the typical scale L (the scale over which the largest possible variation in x_n live), $G_i(\ell)$ is the length of the graph in the i^{th} ℓ–sized interval, and the average is taken over time and different L placements in space. We have seen that $\beta(q)$ depends nonlinearly on q. The numerical results for $\beta(q)$ are given in Table (2.2) for the modified tent map, and in Table (2.3) for the logistic map. For the modified tent map, the $\beta(q)$ values increase with increasing q, except for one critical coupling parameter, $\varepsilon_c = 0.9083$. For this parameter, the scaling indices are found to be nearly the same.

We have defined the q^{th} order structure functions as the differences of the variables $x_n(i)$ separated by a distance ℓ:

$$\left\langle \frac{1}{N_\ell} \sum_i^{N_\ell} |x_{i+\ell} - x_i|^q \right\rangle \sim \left(\frac{\ell}{L}\right)^{q\zeta_q} \tag{5.2}$$

and worked out a relation between the q^{th} order structure functions and the generalized graph dimensions:

$$\beta(q) \leq 2 - \zeta_q \tag{5.3}$$

The numerical results for ζ_q values are given in Table (3.1) for the modified tent map, and in Table (3.2) for the logistic map. For the modified tent map, the scaling exponents tend to zero as q increases. But for the logistic map, we see that although for some values of the parameter λ, there exists a scalin behavior of the structure functions, for other values this scaling breaks down. This shows that the evolution of the system is strongly sensible to the parameters and the graph changes its characteristics at different λ values. When we put the values given in Tables (2.2) and (3.1) in Eq. (5.3), we see that this inequality is satisfied, but not saturated.

To understand how the nonuniformity of the wrinkledness is distributed, we have defined a conserved measure,

$$\mu_i(\ell) = \frac{G_i(\ell)}{G_{tot}} \tag{5.4}$$

where G_{tot} is the length of the graph in an $L-$ sized interval. We have defined the generalized dimensions of the support of the graph, $D(q)$, as

$$\left\langle \sum_i \mu_i(\ell) \right\rangle \sim \left(\frac{\ell}{L}\right)^{(q-1)D(q)} \tag{5.5}$$

The numerical results for $D(q)$ are shown in Table (4.1) for the modified tent map, and in Table (4.2) for the logistic map. We have found that the fractal dimension of the support, $D(0)$, is bigger than the dimension of the set over which most of the measure lives, $D(1)$ [29]. We have also seen that, although in the critical region. there exists a scaling behavior of the q^{th} moments of the measure, there is no such scaling in the pure turbulent region. On the other hand. in the laminar region, $D(q) = D(0) = 1$.

In Tables (4.1) and (4.2), we see that, although within the error bars, $D(q)$ values look the same, they tend to decrease with increasing q for $q > 0$, and to increase for $q < 0$. For the modified tent map, it is interesting to see that the $D(q)$ show a slight change for the critical coupling parameter $\varepsilon_c = 0.9083$. At this value parameter, both the averaged graph length, $< G_\ell^q >$, and the partition function scale better than they do for the other parameters. This critical parameter is an extremum point on the phase transition line, and we believe it deserves more attention.

Since the graph is intermittent, the scaling exponents should vary from one interval to another, so by using a Legendre transform, we obtain

$$f(\alpha(q)) = \alpha q - (q-1)\, D(q) \tag{5.6}$$

The spectrum of $f(\alpha)$ is shown in Figs. (4.6–7). Here, α is the singularity exponent, and $f(\alpha)$ is the dimension of the sets with the singularity exponent α. The slope of the tangent at α_{min} and α_{max} points should in fact be infinite, but while the graphs in Figs. (4.6–7) seemm to go linearly wih a finite slope for large $|q|$. On the other hand, error bars are also mch larger for large $|q|$.

We have also found a relation between the generalized graph dimensions and the generalized dimensions of the support:

$$D(q) = \frac{q}{q-1}\,[\beta(1) - \beta(q)] + 1 \tag{5.7}$$

With the results in Tables (2.2) and (4.1), one can easily see that this relation is numerically satisfied.

Using Eq. (5.3), we can also find a relation between the q^{th} order structure functions and the generalized dimensions of the support:

$$D(q) \leq \frac{q}{q-1}\,(\zeta_q - \zeta_1) + d \tag{5.8}$$

Using the results in Tables (3.1) and (4.1), this equation is seen to be saisfied, but not saturated, as expected.

In summary, we have intrioduced to generalized dimensions, $\beta(q)$ and $D(q)$ for the graph of a scalar function defined over space–time. In place of continous and spatially extended systems, we have taken their discrete time–discrete space analogues, or coupled map lattices. For two different VML, we have demostrated the utility of this generalization, by showing that in the presence of spatio–temporal intermittency, $\beta(q)$ and $D(q)$ behave nonlinearly with q (although within the error bars, we cannot rule out a nonlinear dependence. Most importantly, we have shown that $D(1)$ may indeed be smaller than $D(0)$, so that the dimension of the set over which the bulk of the "wrinkling" of the graph lives, is smaller than that of the support [15].

REFERENCES

[1] MANDELBROT B. B., The Fractal Geometry of Nature, (Fremann, New York, 1982).

[2] HAUSDORFF F., Math Annalen 79, 157 (1918).

[3] BENZI R., PALADIN G., PARISI G. and VULPIANI A., Jour. Phys.A 17, 3521 (1984).

[4] GRASSBERGER P. and PROCACCIA I., Physica D 13, 34 (1984).

[5] HALSEY T. C., JENSEN M. H., KADANOFF L. P., PROCACCIA I. and SHRAIMAN B. I., Phys. Rev. A 38, 1141 (1986).

[6] HENTSCHEL H. G. E. and PROCACCIA I., Physica D 8, 435 (1983).

[7] PALADIN G. and VULPIANI A., Phys. Rep. 156, 147 (1987).

[8] RICHARDSON L. F., Proc. Royal Soc. London, A 110, 709 (1926).

[9] KOLMOGOROV A. N., Docl. Akad. Nauk., USSR 30, 301 (1941).

[10] OBUKHOV A. M., Izv. Akad. Nauk., USSR, Ser. Goegr. Geopiz.

4–5, 453 (1941).

[11] ANSELMET F., GAGNE Y., HOPFINGER E. J. and ANTONIA A. R., J. Fluid Mech. 140, 63 (1984).

[12] MANDELBROT B. B., J. Fluid Mech. 62, 331 (1974).

[13] BENZI R., PALADIN G., PARISI G. and VULPIANI A., J. Phys. A 18, 2157 (1985).

[14] CONSTANTIN P., Commun. Math. Phys. 129, 241 (1990).

[15] CONSTANTIN P. and PROCACCIA I., Phys. Rev. A 46, 4736 (1992).

[16] PROCACCIA I. and CONSTANTIN P., Europhys. Lett. 22, 6891 (1993)

[17] PROCACCIA I. and CONSTANTIN P., Phys. Rev. Lett. 70, 3417 (1993).

[18] CONSTANTIN P. and PROCACCIA I., Phys. Rev. E 47, 3307 (1993).

[19] SREENEVESAN K. R., Annu. Rev. Fluid Mech. 225, 1 (1991).

[20] FALCONER K. J., Geometry of Fractal Sets, (Cambridge Uni. Press, Cambridge, 1985).

[21] KEEKER J. D. and FARMER J. D., Physica D 23, 413 (1986).

[22] KANEKO K., Prog. Theor. Phys. 74, 1033 (1985).

[23] KANEKO K., Prog. Theor. Phys. 99, 263 (1989).

[24] CHATÉ H. and MANNEVILLE P., Phys. Rev. A 38, 4351 (1988).

[25] HOULRIK J. M., WEBMAN I. and JENSEN M. H., Phys. Rev. A 41, 4210 (1990).

[26] CHATÉ H. and MANNEVILLE P., Physica D 32, 409 (1988).

[27] HÜNER M. and ERZAN A., Physica A 212, 314 (1994).

[28] ÇIKCI S., Karmaşık Zaman Serilerinin Analizi, Diploma Thesis, Physics Department, ITU, 1995.

[29] FARMER J. D., OTT E. and YORKE S. A., Physica D 7, 153 (1983).

CURRICULUM VITAE

M. N. Ayşe GORBON graduated from Özel Eseniş Lisesi in 1989, and from Physics Department of Istanbul Technical University in 1993. She is an M.Sc. student in the Physics Program of Istanbul Technical University.